fire

MDPI

Article

Effects of Waste Glass Bottle Nanoparticles and High Volume of Waste Ceramic Tiles on Concrete Performance When Exposed to Elevated Temperatures: Experimental and Theoretical Evaluations

Zahraa Hussein Joudah [1,2], Nur Hafizah A. Khalid [1,*], Hassan Amer Algaifi [3], Akram M. Mhaya [4], Teng Xiong [5], Riyadh Alsultani [6] and Ghasan Fahim Huseien [7,8,*]

1 Faculty of Civil Engineering, Universiti Teknologi Malaysia, Johor Bahru 81310, Johor, Malaysia; zahraa.alsafy85@uomisan.edu.iq
2 Department of Civil Engineering, Faculty of Engineering, University of Misan, Misan 62001, Iraq
3 Institute of Energy Infrastructure (IEI), Universiti Tenaga Nasional, Jalan IKRAM-UNITEN, Kajang 43000, Selangor, Malaysia; hassan.amer@uniten.edu.my
4 Faculty of Civil Engineering and Built Environment, Universiti Tun Hussein Onn Malaysia, Parit Raja, Batu Pahat 86400, Johor, Malaysia; akram@uthm.edu.my
5 School of Built Environment, Faculty of Arts, Design and Architecture, University of New South Wales, Sydney, NSW 2052, Australia; teng.xiong@unsw.edu.au
6 Building and Construction Techniques Engineering Department, College of Engineering and Engineering Techniques, Al-Mustaqbal University, Babylon 51001, Iraq; dr.riyadh.abdulabbas@uomus.edu.iq
7 Guangzhou Institute of Energy Conversion, Chinese Academy of Sciences, Guangzhou 510640, China
8 Department of the Built Environment, School of Design and Environment, National University of Singapore, Singapore 117566, Singapore
* Correspondence: nur_hafizah@utm.my (N.H.A.K.); eng.gassan@yahoo.com (G.F.H.)

Citation: Joudah, Z.H.; Hafizah A. Khalid, N.; Algaifi, H.A.; Mhaya, A.M.; Xiong, T.; Alsultani, R.; Huseien, G.F. Effects of Waste Glass Bottle Nanoparticles and High Volume of Waste Ceramic Tiles on Concrete Performance When Exposed to Elevated Temperatures: Experimental and Theoretical Evaluations. *Fire* **2024**, *7*, 426. https://doi.org/10.3390/fire7120426

Academic Editor: Lizhong Yang

Received: 8 October 2024
Revised: 14 November 2024
Accepted: 19 November 2024
Published: 21 November 2024

Abstract: This article reports the durability performance of modified concrete with silica nanoparticles and a high volume of waste ceramic tiles under varying elevated temperatures. Ordinary Portland cement (OPC) was replaced with 60% waste ceramic tiles powder (WTCPs) and supplemented with 2, 4, 6, 8, and 10% nanopowders from waste glass bottles (WGBNPs) as a rich source of silica. The natural aggregates (both coarse and fine) were fully replaced by the crushed waste ceramic tiles (WTCAs). After 28 days of curing, the modified specimens were exposed to varying elevated temperatures (200, 400, 600, and 800 °C) in a furnace followed by air cooling. Tests such as residual compressive strength, weight loss, ultrasonic plus velocity, visual appearance, and microstructural analysis were conducted. Additionally, analysis of variance (ANOVA) was used to validate the performance of the proposed predictive equations, as well as their terms, using *p*-values and F-values. It was discerned that OPC substitution with WTCPs and WGBNPs significantly improved the concrete's performance under elevated temperatures. It is observed that the addition of 2, 4, 6, 8, and 10% WGBNPs lowered the concrete deterioration by increasing the residual strength and reducing both internal and external cracks. This study provides some new insights into the utilization of WTCPs and WGBNPs to produce sustainable and eco-friendly modified concrete with high spalling resistance characteristics at elevated temperatures.

Keywords: modified concrete; high volume wastes tile ceramic; silica nanoparticles; resistance to elevated temperatures

1. Introduction

Human activities have caused a multitude of environmental issues in recent decades, including water, soil, and atmospheric pollution, in addition to global warming [1–3].

These problems have largely been exacerbated by the cement industry, in which vast quantities of clay, shale, gypsum, and fossil fuels are employed. Furthermore, the industry contributes to approximately 8% of global CO_2 emissions [4,5]. It is estimated that by 2050, the demand of OPC (a broadly used binding agent in the concrete industries) will continue to increase by nearly 6 billion tons [4–6]. It has been determined that one potential method of surmounting the emission of CO_2 emanated by the cement industry is the partial replacement of OPC with agro-industries-originated supplementary cementitious materials (SCMs). These SCMs include fly ash (FA) [7], silica fume (SF) [8], sugarcane bagasse ash (SCBA) [9], ground-granulated blast furnace slags (GBFS) [10], walnut shells ash (WSA) [11], rice husks ash (RHA) [12], limestone powders (LSP) [13], waste papers (WPs) [14], metakaolin (MK) [15], and palm oil fuel ash (POFA) [16]. In recent years, various structural engineering characteristics of these SCMs have been intensively studied to determine whether they would be viable partial replacements for OPC [17–20]. Another important SCM that is employed as a part of an OPC substitute in the production of materials, including mortars, pastes, concretes, high-performance concrete (HPC), pavement concrete, concrete paving blocks, self-compacting concrete (SCC), ultra-high-performance concrete (UHPC), and ultra-high-performance SCC, is ceramic waste [21–23].

Extensive studies in recent years have indicated that ceramic tiles waste (CTW) can be used to replace the various aggregates and cement that constitute concrete. In the present work, the literature related to composites based on cement, including CTW as a potential replacement for aggregates and cement, has been closely examined [24–27]. Moreover, scientific research highlights regarding the physicochemical, mechanical, and durability properties of CTW are investigated [28]. Previous studies have shown that ceramic tiles aggregates (CTA) at specific quantities can be utilized to make concrete in order to make it stronger and more durable [29]. The mechanical and durability performance of concrete can also be enhanced by using materials enriched with high-silica contents like finely ground ceramic tiles powders (CTP) [30,31]. The impacts of CTP addition at various levels in concrete against chemical attack [32–36], drying shrinkage [37], and fire resistance have been evaluated [38]. The academic community is increasingly calling for the implementation of waste materials in concrete, promoting environmental fortification and the creation of sustainable cities and communities [39–42].

Many researchers have examined the post-heating performance of concrete and steel reinforcements. For example, Harada [43] explored the relationship between residual bond strength and temperature by exposing concrete samples to temperatures of up to 450 °C, finding that the residual bond strength was 60% at 100 °C and 10% at 450 °C. Additionally, Royles and Morley [44] found that high temperatures significantly reduced the bond's performance. In the building industries, concrete specialists should ensure proper fire security requirement in the design program [45,46]. Fire is a major life-threatening environmental situation that buildings can face, making it crucial to incorporate proper fire safety measures into building design. These measures, assessed through fire resistance, refer to the time in which a structural component can maintain its integrity and stability and limit heat transfer during a fire [47,48]. Generally, modified concretes prepared with high-aluminosilicate-content materials, such as FA, GBFS, POFA, and WTCPs, have shown significant improvement in concrete performance under elevated temperatures and aggressive environments, such during as sulphuric acid or sulphate attacks [49–51]. The remarkable fire resistance of high-aluminosilicate cement stems from the chemical composition of its constituent materials that are fundamentally inert, possessing low thermal conductivity, high specific heat, and slow rate of strength degradation at rising temperature [52]. These distinct characteristics of concrete recommend it as an efficient barrier to fire in the surrounding areas, protecting it from fire damage [53].

Waste glass had been used to replace cement and conventional aggregates in the production of concrete, and many studies have examined these applications [54–56]. Using waste glass to substitute cement could enhance the sustainability of construction, reduce costs, and reduce CO_2 emissions [57]. Shi and Zheng [58] have examined how waste glass

particle size influences the pozzolanic reaction. In one study by Franco-Luján [59], waste glass particles sized ≤ 45 μm were shown to be viable partial substitutes for OPC, and they had pozzolanic properties. Cementitious compounds (e.g., C–S–H and C–A–S–H) result from the pozzolanic reaction [60–62], and the mechanical properties of cement-based materials are thereby enhanced. The strength activity index (SAI) values of mortars made with 20% waste glass, at 28 days, reveal a significant enhancement in strength performance [63,64]. As per the reported results, the minimum threshold for determining that a SCM has pozzolanic properties was met by the majority of mortars, which had values over 75% [65]. From these findings pertaining to the calcium hydroxide content and SAI of waste glass materials, it appears that waste glass does have pozzolanic properties, though these emerge as more pronounced at the 28-day point of ageing. This makes waste glass similar to a range of alternative SCMs, including FA, SCBA, RHA, and palm oil fuel ash [66–68].

Recent developments in nanotechnology present new possibilities for improving concrete properties by incorporating nano-sized particles [69–71]. Specifically, nano-silica has demonstrated a notable ability to enhance the hydration process [72], contribute to denser microstructures [73], and raise early strength development [74]. In study conducted by Onaizi et al. [75], it was found to incorporate 4–6% WGBNPs, with effective microorganisms significantly improving the early strength development of high-volume fly ash concrete. In another study [6], the WGBNPs were used as an FA-OPC replacement to enhance the bond strength performance of a low-cement binder. From the obtained results, the authors reported that the inclusion of 4% WGBNPs improved the early and late strength properties of the proposed high-volume FA binders. Hamzah et al. [72] used the WGBNPs to enhance the geopolymer mortars durability properties. The authors found that drying shrinkage, porosity, carbonation, and resistance to abrasion and sulphuric acid attack positively improved with the inclusion the WGBNPs in the FA-GBFS matrix. When used alongside ceramic wastes, the use of WGBNPs can help to overcome the limitations related to the early strength development in concrete that are typically associated with most of the pozzolanic material. Research has shown that the presence of WGBNPs in concrete can accelerate the hydration reaction, together with the microstructure density improvement [69]. Results indicate that nano-silica particles act as a nucleation site, facilitating homogeneous and faster production of C-S-H gel, thereby leading to a significant increase in the early strengths of concrete.

Considering the immense importance of various industrial wastes for sustainable concrete development, this study systematically evaluated the combined effect of WTCAs, WTCPs, and WGBNPs (as OPC and natural aggregates substitutes) in modifying various engineering properties (mechanical strength, durability, and microstructures) of the proposed high-performance concrete, rich in high aluminosilicates. The effects of these waste components on the concrete performance under elevated temperatures were accessed. It is asserted that through the optimization of pozzolanic materials' particles size and reactivity, it is possible to enhance the fire resistance of concrete by up to 800 °C, thus promoting broad usage in the construction sectors.

2. Experimental Approaches

2.1. Characterizations Constituent Raw Materials of Concrete

Industrial wastes such as wastes tile ceramic materials (WTCMs) and WGBNPs were utilized as OPC, and natural aggregates (fine and coarse) were substituted to design the proposed concrete specimens. In this study, waste ceramic tiles were sourced from the construction industry. The collected materials were initially cleaned, and only homogeneous ceramic tiles were selected, specifically those with consistent thickness and without any glassy coating. These tiles were then crushed using a jaw crusher and subsequently sieved according to ASTM C33-16 [76]: "Standard Specification for Concrete Aggregates". Ceramic particles passing through a 10 mm sieve but retained on a 4.75 mm sieve were

used as coarse aggregates in concrete specimen preparation. Ceramic particles retained on the 10 mm sieve were further crushed to obtain the desired sizes. Aggregates passing through a 4.75 mm sieve and retained on a 75 μm sieve were utilized as a fine aggregate replacement. Ceramic waste particles passing through the 75 μm sieve were ground in a Los Angeles abrasion testing machine with 20 stainless steel balls, each 40 mm in diameter, for 6 h to produce WTCPs. This ceramic powder was then used as a cement replacement in the formulation of modified cement concretes. The physical and chemical characteristics, microstructures, and morphology of all constituents were determined. The color of OPC was dark greyish with the specific gravity of 3.15, surface area fineness of 3995 cm^2/g, and median particle size of 16.4 μm, wherein 97% of the OPC particles could pass through a 45 μm wet sieve. OPC fulfilled the chemical requirement of ASTM Type I cement as specified in ASTM C150 [77]. Table 1 displays the compositions of OPC with the oxides of calcium (67%) and silica (17%) as its main constituents. It was inferred that OPC containing a high amount of lime can contribute to faster hydration reactions and higher early strength compared to the synthesized ceramic powders.

The particle size (median) of the obtained ceramic powder was estimated to be 17.1 μm, with 97% of the particles being smaller than 45 μm. After six hours of grinding, the size of the particles in the ceramic powders could match those in OPC, thereby meeting the pozzolanic requirements of ASTM C618 [78], which specifies that 66% of the particles must pass through a 45 μm sieve. The BET analysis was conducted to evaluate the physical characteristics of the ceramic powders. The powder exhibited a light gray color, with a surface area of 16.4 m^2/g and a specific gravity of 3.06. The specific gravity, which influences the surface area, was found to be lower than that of the OPC material. The XRF of ceramic powders was recorded to determine their elemental compositions (Table 1). The primary oxide components were silica and alumina, comprising 85.6% of the ceramic content. The levels of silicate, aluminum oxide, and calcium oxide significantly influenced the specimens' synthesis by contributing to the formation of C-A-S-H and C-S-H phases during hydration. A notable 13.2% sodium oxide (Na_2O) content was present in the ceramic chemical composition, which is known to have a strong impact on the hydration process. The loss on ignition (LOI) values in the WTCPs were minimal, aligning with the ASTM C618 standard.

Glass waste bottles were sourced from the food industry. Initially, these bottles were rinsed with tap water to remove any impurities then crushed using a crushing machine. The crushed glass was then sieved through a 600 μm mesh to separate the larger particles. Nanoparticles were prepared via mechanical ball milling, a process based on the principle of using high-energy ball milling to reduce particle size, thus altering the surface properties of the material. To achieve medium particle sizes of ≤25 μm, the sieved glass (maximum weight 5 kg) was processed in a Los Angeles Abrasion Machine with a 25 kg capacity, using sixteen 40 mm stainless steel balls, for a duration of three hours. The resulting powder was then heated at 110 °C (±5) for one hour, followed by an additional grinding for seven hours in a specialized ceramic-ball mill to attain optimal nanoparticle distribution. The nanoscale powder obtained, termed WGBNPs, was subsequently utilized in the preparation of the proposed concrete materials. The median particles size, specific surface areas, and specific gravity of WGBNPs corresponded to 80 nm, 206 m^2/g, and 1.02. Additionally, the surface morphology of the concrete revealed significantly higher silica than OPC and ceramic powders. Table 1 shows the chemical compositions of WGBNPs as obtained from XRF measurement. The oxides of aluminum and silica were the major components of WGBNPs (making up to 83%). Moreover, the WGBNPs demonstrated lower loss on ignition (LOI) values, which align with the standards outlined in ASTM C618.

Table 1. Chemical compositions of OPC, WTCPs, and WGBNPs, obtained via XRF measurement.

Composition and LOI	OPC	WTCPs	WGBNPs
SiO_2	17.60	71.7	69.14
Al_2O_3	4.53	13.89	13.86
Na_2O	0.13	13.21	8.57
Fe_2O_3	3.35	0.36	0.24
CaO	67.84	0.02	3.16
MgO	2.18	0.64	0.68
K_2O	0.27	0.03	0.01
SO_3	2.10	0.01	4.10
Others	0.27	0.01	0.08
LOI	1.73	0.13	0.16

Contaminants-free crushed WTCAs were utilized as fine and coarse aggregates to replace the natural aggregates (river sand and crushed granite stone) and make the proposed mix design. These aggregates were stored under saturated surface dry (SSD) conditions, reducing the moisture contents in the specimens. Sieve analyses (Figure 1) of the WTCAs as coarse aggregates were conducted following the stipulation of ASTM C136 [79]. As coarse aggregates, the WTCAs' specific gravity, highest size of particle, and rate of water absorption were 10 mm, 2.36, and 1.4%, respectively (in accordance with ASTM C127 [80]), compared to 10 mm, 2.67, and 1.2% for natural coarse aggregates. Additionally, the natural aggregate was replaced by coarse waste ceramic particles, meeting the requirements of ASTM C33.

The concrete mixes were designed using WTCAs as fine aggregate that met the standards. Similarly, ceramic waste was crushed and sieved to meet ASTM C33 requirements, making it a viable replacement for river sand in the proposed concrete mixtures. Following ASTM C128 standards, the specific gravity and water absorption ability of the WTCAs fine aggregates were also measured in SSD form [81]. The processed fine WTCAs were graded well, with a maximum size of 4.75 mm, indicating its suitability for the concrete mixture.

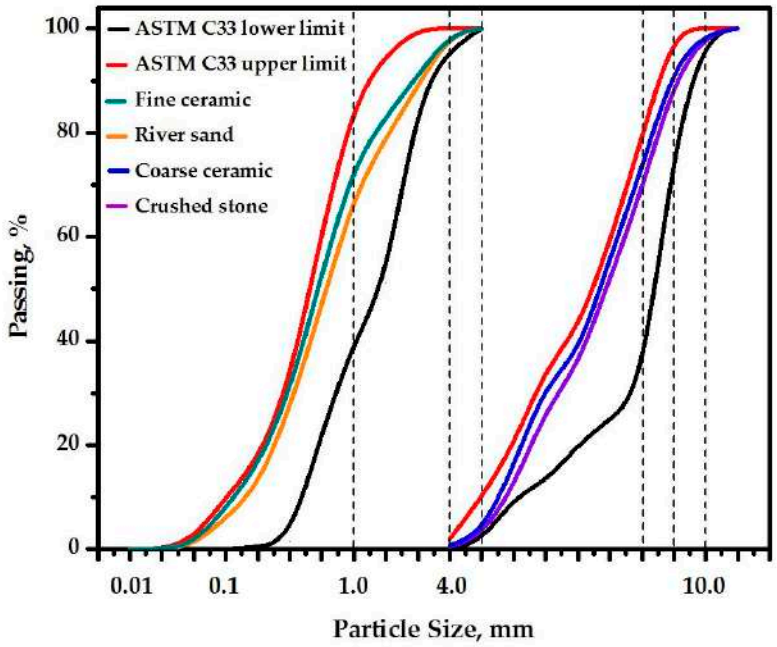

Figure 1. Results of sieve analysis for sand, crushed stones, and fine and coarse aggregates of ceramic waste according to ASTM C33.

2.2. Fabrication of Mix Designs

Table 2 outlines the modified sustainable mixes containing amounts of WGBNPs-derived nanosilica with enhanced hydration reaction and microstructures. The resultant mixture included WTCPs (252 kg/m^3) and OPC (168 kg/m^3), along with specified aggregate proportions, water-binder ratios (w/b), and superplasticizer (SP). The content of WGBNPs ranged from 2 to 10% of the total binder content. The performance of the proposed modified concrete was assessed through extensive testing, including compressive strength, splitting tensile strength, and flexural strength tests, as well as X-ray diffraction (XRD), differential thermogravimetric analysis (TGA-DTG), and field emission scanning electron microscopy with energy dispersive X-ray (FESEM-EDX) measurements.

All the obtained binders composed of OPC, WTCPs, and WGBNPs were mixed homogeneously for 3 min in a mechanical blending machine (0.2 m^3 capacity), producing the desired concrete. Initially, for 2 min, the aggregates (fine and coarse) were blended, followed by the addition of the other 50% (blended for an extra 3 min at dry conditions). Subsequently, the ternary blended binder (OPC-WTCPs-WGBNPs) was introduced. All materials, including the binder and aggregate, were blended in dry conditions for an additional 5 min followed by water and SP activation. Lastly, the obtained mixture was blended for an extra 4 min, followed by the measurement of the slump values. The obtained mixes were dispensed in pre-made steel molds according to the ASTM C579-18 standards [82]. Workability was assessed through a slump test in accordance with ASTM C143 [83].

The concrete specimens were prepared in cubical-shaped (100 mm × 100 mm × 100 mm) pre-cleaned (free of any residues) molds in accordance with the corresponding standards of BS 1881-108 [84]. The designed mixes were dispensed in the molds as compacted layer by layer, wherein the compaction of each one was performed on a vibration table, ensuring the minimization of air trapping. A plasterer float was used to label the obtained mix surface on mold. The concrete mixes were kept in laboratory conditions at a temperature of 26 °C ± 1.5 and a relative humidity of 75% for 24 h, followed by demolding and water-curing for a week. The procedure for the preparation of the proposed concrete specimens is presented in Figure 2.

Table 2. Concrete mix containing 60% WTCPs as an OPC substitute and a varying level of WGBNPs.

Phase	Mix Codes	Mixtures	Binder, kg/m^3			Waste Ceramic, kg/m^3		W/B	SP, %
			OPC	WTCPs	WGBNPs	Fine	Coarse		
Control sample	OPC	100% OPC	420	0	0	816	894	0.48	1.5
High-volume WTCPs	60WCP	60% WTCPs	168	252	0				
Effect of WGBNPs (2, 4, 6, 8, and 10%)	2NPs	2% WGBNPs	168	252	8.4				
	4NPs	4% WGBNPs			16.8				
	6NPs	6% WGBNPs			25.2				
	8NPs	8% WGBNPs			33.6				
	10NPs	10% WGBNPs			42				

Figure 2. Proposed concrete specimens' preparation procedure.

2.3. Tests Procedure

To evaluate the modified concrete specimens' resistance to varying elevated temperatures of 200, 400, 600, and 800 °C, cubes with a size of 100 mm × 100 mm × 100 mm were cast. After 4 weeks of age, the concrete specimens were subjected to tests using an automatic furnace, according to ASTM E119 standard [85] (Figure 3). For each heating stage, three cubical samples were examined to calculate the mean value. Before subjecting the specimens to elevated temperatures using the furnace, the weight, UPV readings, and visual appearance were assessed, as shown in Figure 4. In accordance with ASTM C109 [86], the compressive strength (CS) test was carried out. For the CS, three cubes' specimens were tested at 28 days, and the average value was considered as a reference to measure the residual strength after heating. After each stage of heating (Table 3), the residual CS (RCS) was assessed to measure the deterioration in proposed performance in aggressive environments.

After exposure to the heat, modified concrete specimens were cooled using an air cooling method at a lab temperature of 27 °C ± 3. The weight of the tested specimens after the exposure to varying elevated temperature were evaluated to determine the loss of weight. In accordance with the ASTM C597 standard [87] for ultrasonic pulse velocity (UPV), the relative quality and visual appearance of the specimens were evaluated after exposure to heat. Subsequently, the concrete specimens underwent CS tests to determine both the RCS and strength loss percentage. Furthermore, the microstructures of the specimens were analyzed through various tests, including XRD, FESEM-EDX, TGA-DTG, and FTIR measurements. For the XRD, TGA-DTG, and FTIR tests, paste specimens were prepared for this purpose and tested under similar conditions. The XRD analysis was completed at the 2theta range of 3–90°, with a step size of 0.02° and a scan speed of 0.5 s/step. The samples were mounted on a brass stub sample holder and secured with carbon tape. After being dried under infrared radiation for 5 min, they were coated with a gold layer using a blazer sputtering coater. Images were captured at 20 kV with 1000× magnification to observe the patterns.

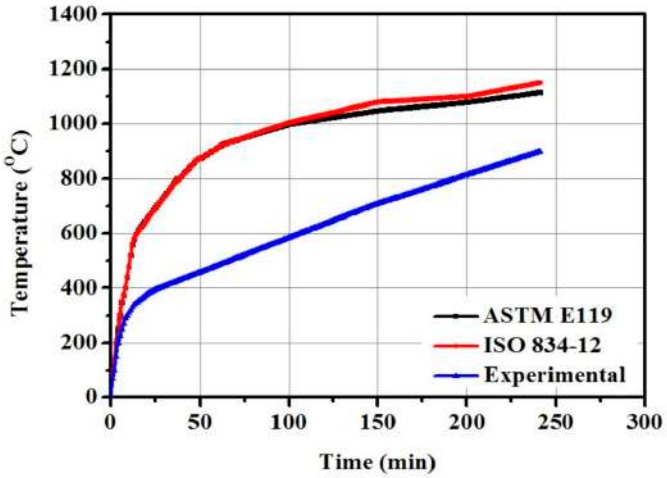

Figure 3. Variation of temperatures against time based on ASTM E119 [85] and ISO 834-12 [88].

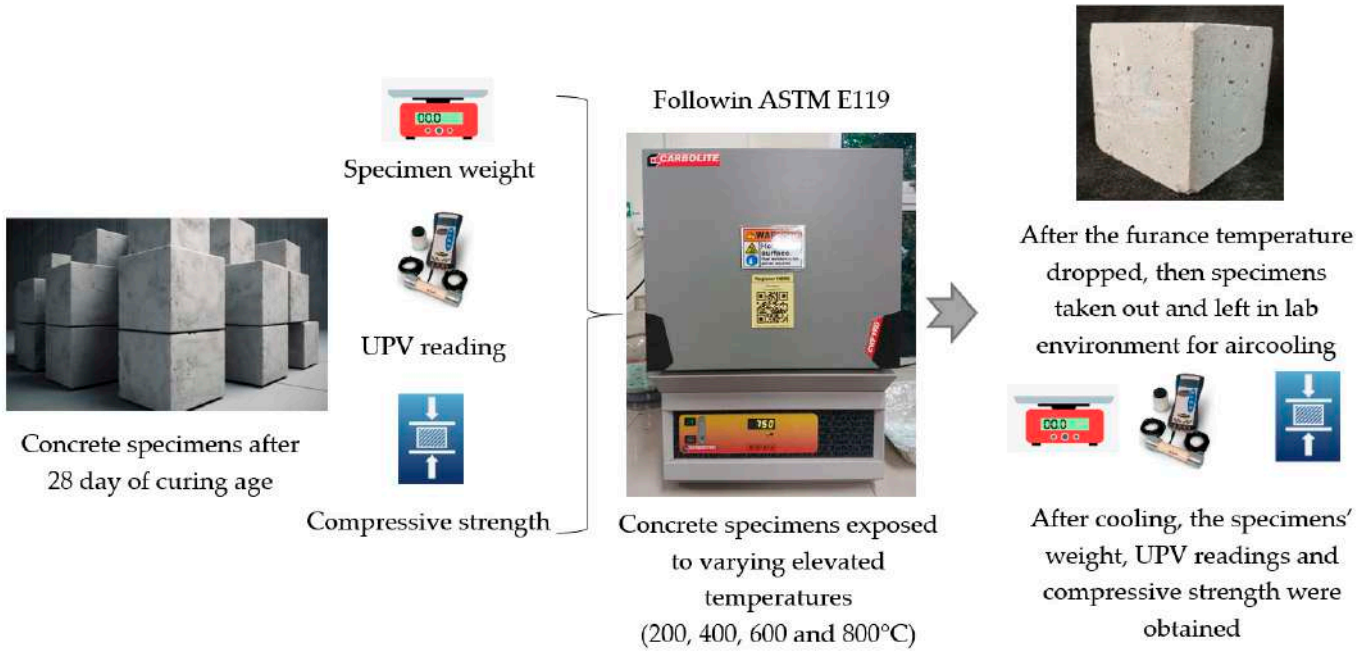

Figure 4. Heating and cooling procedure following ASTM E119 [85].

Table 3. Specimens' sizes, heating, and cooling times.

No.	Temperature, °C	Specimens' Details		Time, Minutes		
		Size, mm	Number	Heating	Furnace Drop Temperature	Cooling in the Lab Condition
1	27 (control specimens)	100 × 100 × 100	3	0	0	0
2	200	100 × 100 × 100	3	15	10	60
3	400	100 × 100 × 100	3	45	30	150
4	600	100 × 100 × 100	3	95	60	240
5	800	100 × 100 × 100	3	195	120	360

2.4. Theoretical Approach

Response surface methodology (RSM) was used to assess the performance of the concrete mixes enclosing a high level of WTCPs and WGBNPs when exposed to various elevated temperatures. Specifically, the face-centered central composite design (FC-CCD), a

technique within the RSM approach, was utilized for its simplicity and accuracy in the current study. FC-CCD has been extensively used in the literature to mathematically study the interaction and relationship between dependent and independent variables [89]. WGBNPs and temperature were considered as independent variables, while strength loss, weight loss, and UPV were the dependent variables. Several sequential steps were taken to develop the RSM model. In the first step, nine experimental tests were conducted using Equation (1). These tests were designed according to the basic concept of FC-CCD, which involves three groups of experimental tests: factorial, axial, and central groups. Here, m and n refer to the number of central experimental tests and the number of independent variables, respectively, while Q represents the total number of required experimental tests. Table 4 presents the number and values of the nine experimental tests as well as their coded values.

$$Q = 2^n + 2n + m \tag{1}$$

Table 4. The required experimental test to develop the RSM model.

No.	Real Values		Codded Value		Groups
	WGBNPs, %	Temperatures, °C	X_1	X_2	
1	6	500	0	0	Central values
2	10	500	1	0	Axial values
3	6	200	0	−1	Axial values
4	6	800	0	1	Axial values
5	6	500	0	0	Axial values
6	10	800	1	1	Factorial values
7	2	200	−1	−1	Factorial values
8	2	800	−1	1	Factorial values
9	10	200	1	−1	Factorial values

In the second phase, the gathered experimental data were analyzed using Design Expert software, version 13 (DX13). The relationships between the dependent and the independent variables were modeled using a quadratic equation (Equation (2)), where α_o denotes the intercept, α_i represents linear effect coefficients, α_{ii} refers to quadratic effect coefficients, and α_{ij} serves as the interaction effect coefficient. In addition, Y_i and X_i represent the dependent and independent variables. Subsequently, the performance of the developed equation was examined through the coefficients of determination (R^2) and mean absolute percentage error (MAPE), as shown in Equations (3) and (4) [90,91]. The former evaluates the strength and the closeness between the real and estimated results, while the latter is widely used to assess the accuracy and reliability of the equation. In these equations, r refers to the number of experiments, and the averages of the estimated and actual experimental results are denoted by $\overline{Y}$ and $\overline{X}$, respectively.

$$Y_i = \alpha_o + \sum_{i=1}^{2} \alpha_i X_i + \sum_{i=1}^{2-1} \sum_{j=2}^{2} \alpha_{ij} X_j X_i + \sum_{i=1}^{2} \alpha_{ii} X_i^2 \tag{2}$$

$$Y_i = \left(\frac{\sum_1^r \left(X - \overline{X}\right)\left(Y - \overline{Y}\right)}{\sqrt{\sum_1^r \left(X - \overline{X}\right)^2 \sum_i^r \left(Y - \overline{Y}\right)^2}} \right)^2 \tag{3}$$

$$MAPE = \frac{1}{r} \sum_{i=1}^{r} \left| \frac{Experimental - Estimated}{Experimental} \right| * 100 \tag{4}$$

3. Results and Discussion

3.1. Fresh Concrete' Slump Values

The influence of incorporating high volumes of WTCPs and silica nanoparticles (WGBNPs) on the workability of fresh concrete was assessed in accordance with ASTM C143 [83]. The findings reveal that replacing OPC with 60% waste ceramic powder significantly reduced the concrete workability by 18.95%, decreasing the slump readings from 190 mm to 154 mm. This reduction is attributed to the porous and irregular structure of ceramic particles, which increases water demand and subsequently diminishes concrete workability. Similarly, incorporating WGBNPs in the high WTCPs-OPC matrix slightly reduced the workability (Table 5). As WGBNPs content increased from 0% to 2%, 4%, 6%, 8%, and 10%, the concrete slump reading decreased by 3.24%, 7.79%, 10.38%, 14.28%, and 16.88%, respectively. The observed reduction in the flowability of the proposed concrete is associated with the high specific surface area of WGBNPs, which increases water demand, raises concrete viscosity, and lowers slump values.

Table 5. Slump and compressive strength of modified concrete.

Tests	OPC	WTCPs	WGBNPs				
	100%	60%	2%	4%	6%	8%	10%
Slump, mm	190	154	149	143	138	132	126
Compressive strength, MPa	43.9	26.3	28.3	36.9	35.3	31.1	26.9

3.2. Compressive Strength Development

Table 5 illustrates the effect of different silica nanoparticle concentrations derived from WBGNPs on the compressive strength of concrete over time. The inclusion of WBGNPs at levels of 2%, 4%, 6%, 8%, and 10% in a high-volume WTCPs mix (60%) consistently enhanced both early and long-term compressive strength. At 28 days, specimens containing these nanoparticle concentrations reached compressive strengths of 28.3, 36.9, 35.3, 31.1, and 26.9 MPa, all surpassing the compressive strength of the high ceramic mixture (26.4 MPa). This improvement is credited to the nanoscale particles' ability to accelerate hydration, enhance gel density, reduce porosity, and refine the concrete's microstructure [92–97]. Overall, incorporating nanomaterials in modified concrete enables filling and micro-aggregate effects, fostering the formation of cementitious materials and yielding a denser matrix [98,99].

3.3. Loss on Weight

The effects of heating on the specimens' weight loss were evaluated at varying temperatures of 200, 400, 600, and 800 °C. For all tested specimens, the weight loss percentage slightly increased with the increasing exposure temperatures. Figure 5 shows the obtained results of four types of modified concrete compared to control specimens of OPC. For the control specimens (OPC), the increasing elevated temperature from 27 °C to 200, 400, 600, and 800 °C resulted an increase in weight loss of 1.7%, 5.1%, 8.8%, and 12.2%, respectively. However, the replacing 60% OPC with WTCPs significantly improved the durability performance and reduce the weight loss percentage to 1.4%, 3.9%, 6.3%, and 9.6%. More enhancement on resistance of modify concrete was observed with an additional 4% WGBNPs in the high-volume WTCPs-OPC matrix. The weight loss dropped to 1.2%, 3.2%, 6.1%, and 9.1%, as shown in Table 6. The specimens containing 6% WGBNPs and exposed to 200, 400, 600, and 800 °C displayed somewhat better performance than others and achieved weight loss of 1.1%, 2.9%, 5.8%, and 8.9%, respectively. The obtained higher performance of concrete modified with WTCPs of 60% and WGBNPs of 4–6% can be attributed to the high content of aluminosilicate, which has shown higher stability under elevated temperatures compared to the high-calcium-content control specimens.

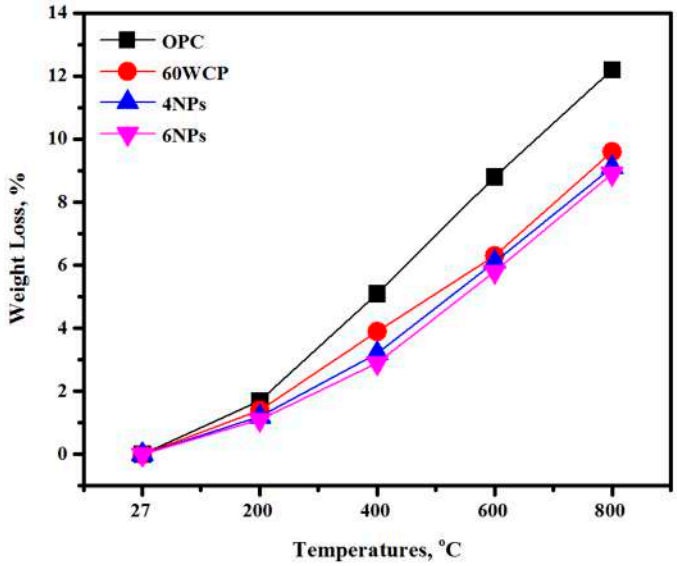

Figure 5. Loss on weight of the designed mixes containing a high level of waste ceramic tiles powder and WGBNPs exposed to elevated temperatures.

Table 6. Effects of elevated temperatures on weight loss percentage, RCS, and UPV readings of the proposed concretes.

Tests	Temperature, °C	OPC 100%	WTCPs 60%	WGBNPs 4%	WGBNPs 6%
Weight loss, %	0	0	0	0	0
	200	1.7	1.4	1.2	1.1
	400	5.1	3.9	3.2	2.9
	600	8.8	6.3	6.1	5.8
	800	12.2	9.6	9.1	8.9
Residual strength (RCS), MPa	0	43.9	26.4	36.9	35.3
	200	42.01	25.4	35.7	34.2
	400	29.9	22.6	32.5	31.7
	600	16.1	15.9	23.9	23.1
	800	10.49	9.34	13.68	13.27
UPV readings, m/s	0	4480	3692	4410	4376
	200	4436	3680	4396	4352
	400	4152	3446	4236	4210
	600	3520	3084	3766	3790
	800	2236	2410	2488	2604

3.4. Residual Compressive Strength

Figure 6 illustrates the effect of heating on the RCS of modified concrete. At 28 days of age, the modified concrete' specimens were exposed to 200, 400, 600, and 800 °C. For each mixture at varying temperatures, three cubes of concrete were tested, and the average value was considered. For all the tested specimens, the deterioration and strength loss trend to increase with increasing exposure temperatures. For the control specimens, the temperature increasing from 27 to 800 °C reduced the corresponding CS values from 43.9 to 10.5 MPa. Conversely, the CS value for the mix made with 60% WTCPs as a replacement for OPC decreased from 26.4 MPa to 24.4, 22.6, 15.9, and 9.3 MPa. Specimens of high-volume ceramic containing 4% WGBNPs showed similar trend of results, and the strength value dropped from 36.9 MPa to 35.7, 32.5, 23.9, and 13.7 MPa, and from 35.3 MPa to 34.2,

31.7, 23.1, and 13.3 MPa for the specimens prepared with 6% silica nanoparticles, as shown in Table 6.

The highest loss in CS with more deterioration at varying elevated temperatures was observed with the control specimens of OPC (Figure 7). However, the inclusion of 60% WTCP and 4 to 6% WGBNPs significantly improved the concrete performance under heating. Concrete specimens designed with 60% WTCPs as a replacement for OPC and the addition 6% WGBNPs achieved the highest resistance under varying elevated temperatures compared to other specimens. At 200 °C, the loss in strength slightly decreased from 4.3% to 3.6, 3.3, and 3.1% with the inclusion of 60% WTCPs and 4% and 6% WGBNPs, respectively. At 400 °C, a sharp improvement in the resistance of the specimens was observed with the inclusion of WTCPs and WGBNPs, but the loss% decreased from 31.9% to 14.4, 11.8, and 10.1%. A similar trend was observed at 600 and 800 °C, and the loss in strength dropped from 63.4% and 76.1% to 34.6% and 62.4% with the inclusion of 60% WTCPs and 6% WGBNPs in the OPC matrix.

At the first stage of test, the small range in loss strength was observed when increasing the temperature from 27 °C to 200 °C, attributed to the absorbed and free water evaporation. However, there was a repaid increment in strength loss of the OPC specimens when increasing the temperature from 200 °C to 400 °C due to the decomposition of Portlandite ($Ca(OH)_2$) into calcium oxide (CaO) and water (H_2O) and the escape of the chemically bound water and decomposed water [100]. Finally, high deterioration and a sharp loss in strength with more internal and external cracks were observed when increasing the temperature from 400 °C to 600 °C and 800 °C, which is chiefly ascribed to the degradation of Portlandite and calcium (aluminum) silicate hydrate (C-(A)-S-H).

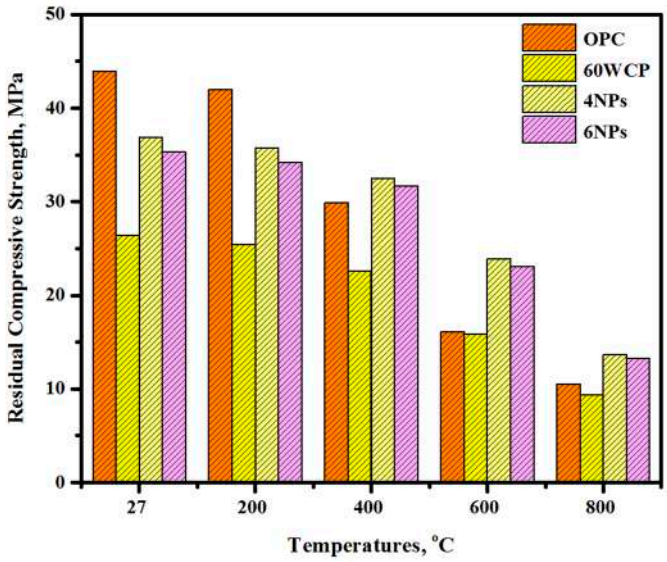

Figure 6. RCS of the designed mixes containing high-volume tile ceramic wastes and WGBNPs exposed to varying elevated temperatures.

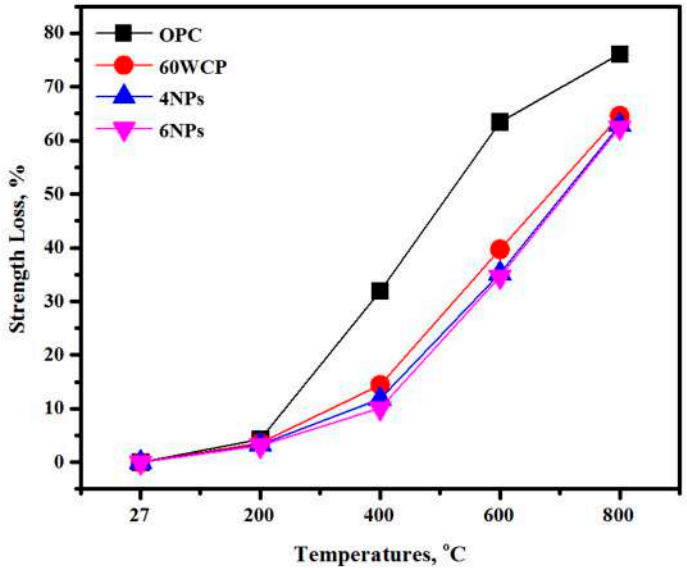

Figure 7. Strength loss percentage of proposed concrete containing high-volume tile ceramic wastes and WGBNPs exposed to elevated temperatures.

3.5. Ultrasonic Pulse Velocity

Figure 8 shows the residual UPV reading after the modified concrete specimens exposed to varying elevated temperatures (200, 400, 600, and 800 °C). For all the tested specimens, the increasing exposure temperature from 27 °C to 800 °C resulted in a decrease in UPV reading. A small change in UPV readings was observed at a low temperature of 200 °C. However, the specimens exposed to 600 and 800 °C displayed lower performance and showed significant changes in UPV readings. Among the four tested mixtures, a higher deterioration was observed for the control specimens. The increasing exposure temperature from 27 °C to 200, 400, 600, and 800 °C led to a drop in the UPV reading from 4480 m/s to 4436, 4152, 3520, and 2236 m/s, respectively. However, replacing 60% OPC with WTCPs positively improved the concrete performance, increasing the specimens' resistance to elevated temperatures. The results presented in Table 6 show that the specimens prepared with a high amount of WTCPs and exposed to elevated temperatures have higher performance; the UPV readings dropped from 3692 m/s to 3084 and 2410 m/s when increasing the elevated temperature from 27 °C to 600 and 800 °C, respectively. A similar trend in the results was found for the modified concrete specimens prepared with 4 and 6% WGBNP; significant improvement was observed with a lower loss in UPV readings. The results indicate that the increasing exposure temperature from 27 °C to 600 and 800° resulted in a decrease in UPV readings from 4410 m/s to 3766 and 2488 m/s for 4% WGBNPs and from 4376 m/s to 3790 and 2604 m/s for the 6% WGBNPs. It is well known that increasing the exposure temperatures to 200, 400, 600, and 800° leads to high water evaporation, $Ca(OH)_2$ decomposition, the formation of C-(A)-S-H gel, more pores, and larger internal cracks. The high deterioration of the concrete's surface leads to lower UPV readings.

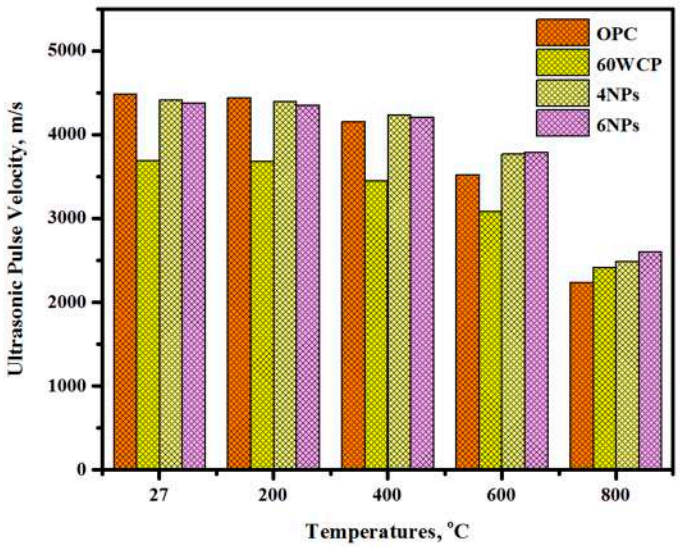

Figure 8. UPV readings of the specimens containing high levels of waste ceramic tiles and WGBNPs exposed to elevated temperatures.

3.6. Visual Appearance and Impact of Temperature Rise on Cracks

The effects of an elevated temperature of 800 °C on the surface, cracks number, and width of the tested concrete specimens were evaluated. Figure 9 highlights the surface cracks of the OPC and modified concrete specimens with high-volume WTCPs contents (60%) incorporating varying WGBNPs (4 and 6%) after exposure to 800 °C. Control specimens, which were prepared with only OPC as a binder, showed lower performance under heating compared to other specimens. Compared to concrete specimens and those designed with WTCP or/and WGBNPs, wider cracks were observed in the surface of OPC specimens exposed to 800 °C (Figure 9a). As shown in Figure 9b, replacing 60% OPC with WTCP slightly reduced the deterioration of the concrete surface. A similar trend was observed, for the inclusion of 4% and 6% WGBNPs, which significantly improved the concrete durability under the heating. The addition 4% and 6% WGBNPs enhanced the resistance of the tested specimens and reduces the width and number of cracks on the surface, as shown on Figure 9c,d. The heating process is commonly associated with several changes, such as moisture evaporation, internal vapor pressure buildup, fine aggregate expansion, cement paste contraction, and chemical decomposition. When subjected to elevated temperatures, concrete undergoes significant changes in both its chemical composition and its physical structure. Above approximately 110 °C, dehydration processes, including the release of chemically bound water from calcium silicate hydrate (C-S-H), become prominent. This dehydration, combined with the thermal expansion of aggregates, generates internal stresses, leading to the formation of microcracks within the material, starting at around 300 °C. Calcium hydroxide [$Ca(OH)_2$], a critical component of cement paste, dissociates near 530 °C, contributing to the shrinkage of the concrete structure. When fires are extinguished using water, calcium oxide (CaO) reacts to form [$Ca(OH)_2$], which exacerbates cracking and accelerates the crumbling of the concrete [101]. Consequently, the effects of high temperatures typically manifest as surface cracking and spalling. C-S-H gel, the primary strength-contributing compound in cement paste, begins to decompose at temperatures exceeding 600 °C. By 800 °C, concrete typically disintegrates, and at temperatures above 1150 °C, feldspar melts while other minerals in the cement paste transition into a glass phase [102]. Consequently, significant microstructural alterations occur, leading to a substantial loss of strength and durability in the concrete. Both concrete color and other characteristics, like density and thermal resistivity, were consid-

erably influenced by the change in chemical contents, especially with respect to the formulation of more hematite and nepheline under elevated temperatures, which affected the concrete's strength and physical characteristics [103,104].

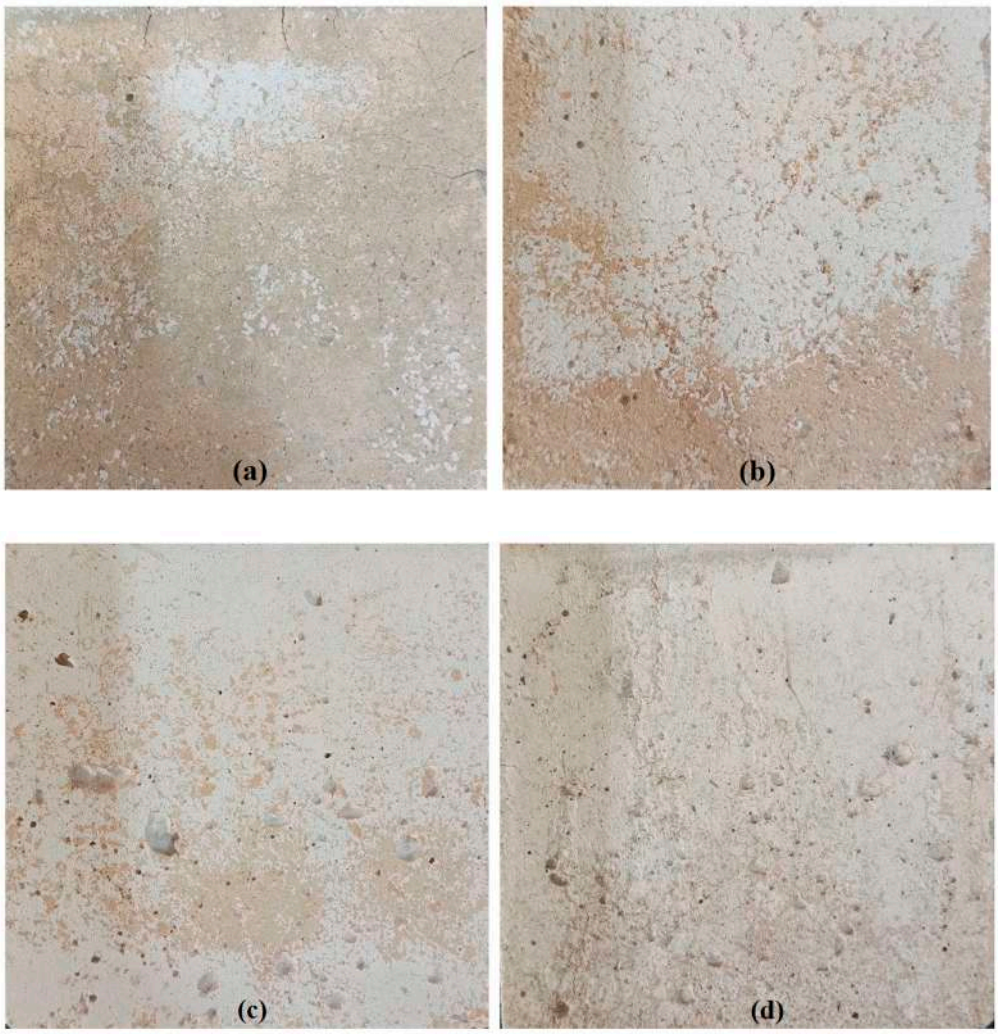

Figure 9. Visual appearance of modified concrete containing a high volume of waste ceramic tiles and WGBNPs after exposure to elevated temperature: (**a**) 100% OPC; (**b**) 60% WTCPs; (**c**) 4% WGBNPs; (**d**) 6% WGBNPs.

3.7. Impact of Temperature Rise on Discoloration

The heating-dependent color changes of modified concrete with WTCPs and WGBNPs were evaluated. Figure 10 shows the influence of heating (800 °C) on the tested concrete specimens' color. The increasing temperature from 27 °C to 800 °C led to a color change from light to dark grey when increasing the level of OPC substitution by WTCPs and WGBNPs, which was retained until 400 °C. With the further increase in temperature at 400 °C, the color of the concrete shifted slightly to a vanilla shade. However, at 800 °C, it turned into a light grey-white color. The burning effect was more intense on the external surfaces and gradually decreased toward the interior, leading to most of the observed changes. Detailed observations of the crushed specimens showed that the surface color at a given temperature penetrated the concrete, depending on the inward heat intensity. In addition, a noticeable discoloration of the specimen's surface was found to extend up to nearly 10 mm deep, mainly for the concrete subjected to 600 °C or lower, which differed in the mixes exposed to 800 °C. The obtained findings are consistent across all modified

concrete mixes containing WTCPs and WGBNPs. Concrete is a composite material composed of aggregates, cement, and water. Consequently, the type and characteristics of the aggregate and cement significantly influence the properties of concrete when exposed to elevated temperatures. The color changes, internal and surface cracks, and strength deterioration of the concrete with varying cement compositions and aggregates differ under high-temperature conditions, primarily due to the mineral composition of the cement and aggregates. For instance, quartz, in ceramic aggregates, undergoes a polymorphic transformation at 570 °C, where quartz α converts to quartz β, leading to volume expansion and structural damage [103,104]. Additionally, the extent of the color change in heated concrete is closely associated with the type of aggregate used in its composition. It is widely recognized that concrete containing siliceous aggregates, such as quartz and flint, exhibits a red hue when heated to temperatures between 300 °C and 600 °C. Furthermore, the cement matrix changes color depending on the temperature: it becomes whitish-gray at 600 °C to 900 °C and shifts to a buff color when heated between 900 °C and 1000 °C [103,104]. These temperature-induced color changes in construction concrete are readily identifiable through visual comparison with unheated concrete.

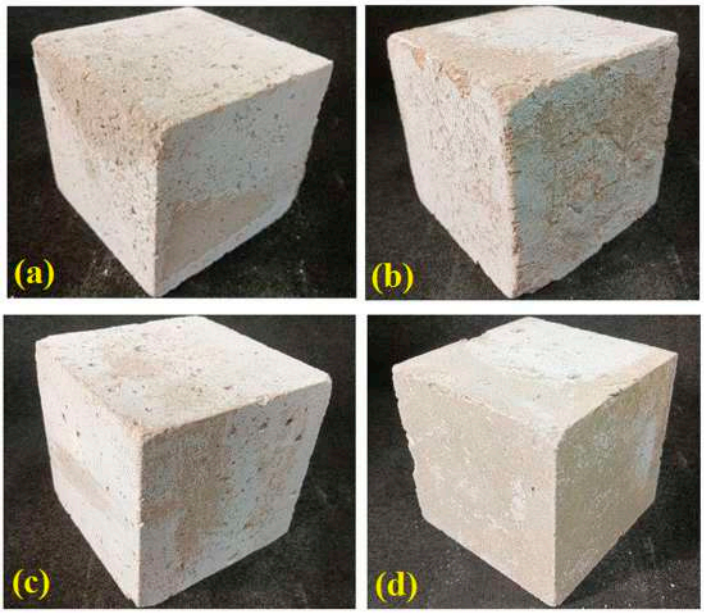

Figure 10. Discoloration of modified concrete containing a high level of waste ceramic tiles and WGBNPs exposed to elevated temperatures: (**a**) 100% OPC; (**b**) 60% WTCPs; (**c**) 4% WGBNPs; (**d**) 6% WGBNPs.

3.8. Scanning Electron Microscopy (FESEM)

The effects of heating on the surface morphology of modified concrete specimens exposed to 800 °C were evaluated. Figures 11–14 illustrate the change in surface morphology of 60% OPC, 4% WTCP, and 6% WGBNPS concrete specimens, respectively. All the obtained results from the FESEM test after exposure to heat were compared to the surface morphology of specimens before heating exposure. The tested specimens of the proposed concrete showed significant change in surface morphology after being heated to 800 °C; the rough surface, pores, and cracks sharply increased; and the deterioration clearly appeared. In Figure 11, the control specimens prepared with only the OPC binder showed greater deterioration in the surface than other samples containing WCP and WGBNPs binders. The specimens designed with low OPC content that was replaced by WTCPs and WGBNPs showed similar outcomes, wherein the number of cracks and pores increased with the increasing exposure temperatures (Figures 12–14). Specimens prepared with lower OPC content showed better performance compared to control specimens.

It is well know the elevated temperatures negatively affect concrete durability by generating micro-cracks and causing pore enlargement, and this is attributed to hydration reaction-mediated products and intense water loss. These findings suggested that the obtained specimens cannot withstand the elevated temperature-induced extreme heat stress, resulting in reduced CS. With a further increase in temperature, the coarse aggregate in the concrete begun to degrade thermally, producing cracks, spalling, and a decrease in CS [105]. After exposure to 800 °C, considerable deterioration and damage to the concrete microstructures were observed [106]. Extensive cracking and the formation of large pores were noted, suggesting substantial degradation of the concrete microstructure because of accelerated dehydration and the transition from disordered to ordered structures, thus contributing to CS decrease [107].

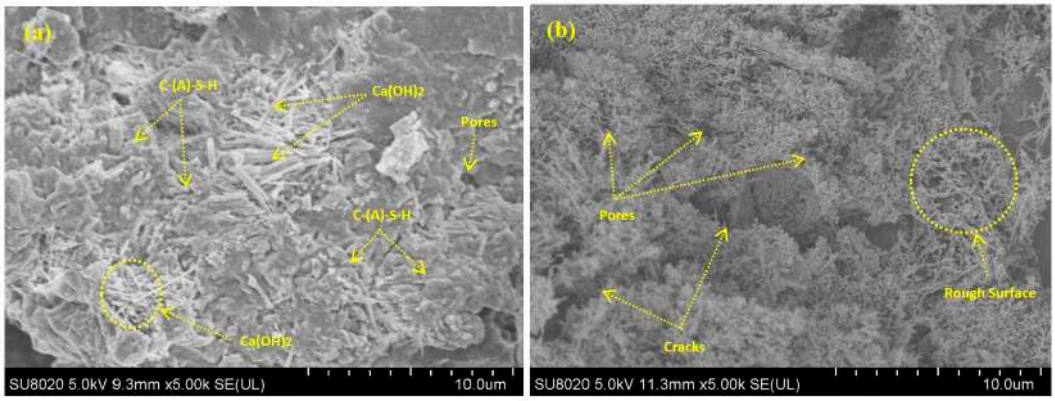

Figure 11. FESEM images of 100% OPC (**a**) before and (**b**) after heat exposure at 800 °C.

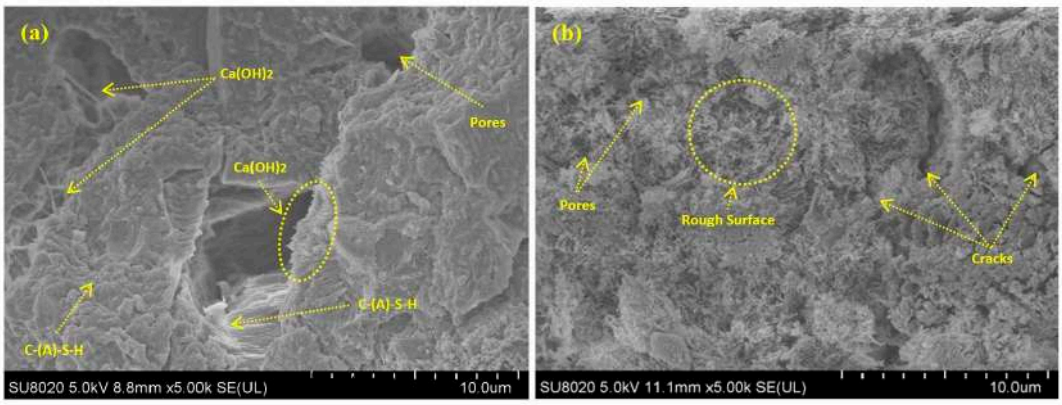

Figure 12. FESEM images of 60% WTCPs (**a**) before and (**b**) after heat exposure at 800 °C.

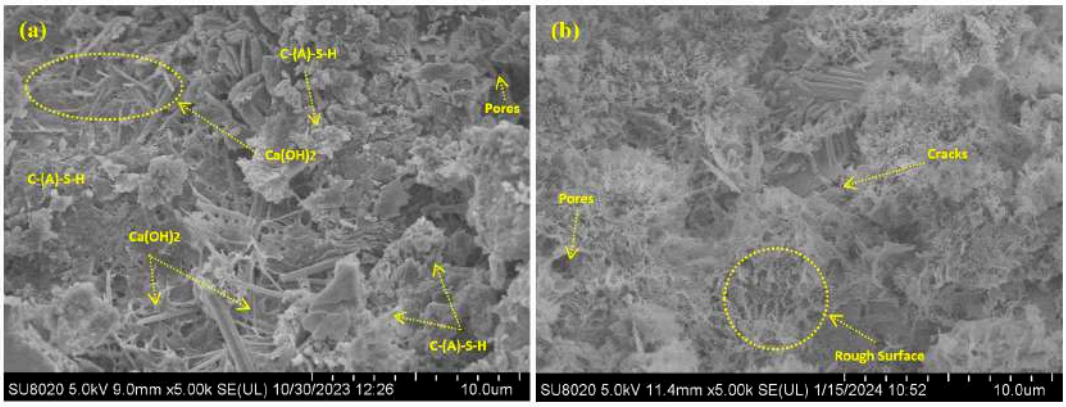

Figure 13. FESEM images of 4% WGBNPs (**a**) before and (**b**) after heat exposure at 800 °C.

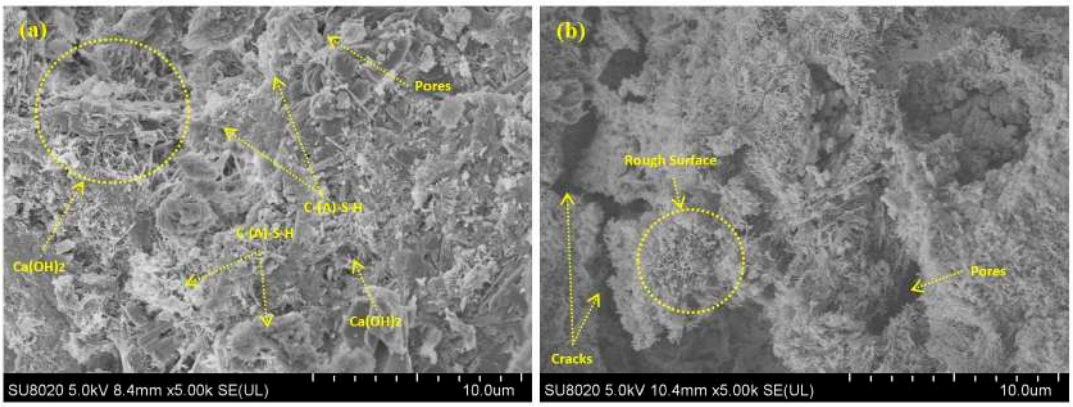

Figure 14. FESEM images of 6% WGBNPs (**a**) before and (**b**) after heat exposure at 800 °C.

3.9. Energy Dispersive X-Ray Analysis (EDX)

The EDX spectra of the control specimen (OPC) and the optimal mixtures prepared with 60% WTCP and 4% WGBNPs were recorded. The obtained results for EDX are presented in Figures 15 and 16. The content of Ca, Si, Fe, Al, Mg, S, K, and Na were found to be 39%, 6.6%, 2%, 1.9%, 1.1%, 1%, 0.1%, and 0.1% for the OPC specimens (Figure 15) and 21.2%, 11.5%, 3.3%, 1.2%, 0.8%, 0.5%, 0.3%, and 0.3% for the 4% WGBNPs specimens (Figure 16), respectively. The high content (39%) of Ca for the OPC specimens compared to the lower Ca content (21.2%) of the 4% WGBNPs specimens was attributed to the water evaporation in Portlandite ($Ca(OH)_2$) and dense gels of C-S-H and C-A-S-H, which explained the lower CS performance of OPC specimens under the heating [108,109]. Furthermore, the high content of Si (11.5%) for the 4% WGBNPs specimens compared to 6.6% was observed with OPC specimens, contributing to the high thermal stability of modified cement with WTCPs and WGBNPs under elevated temperatures.

(**a**)

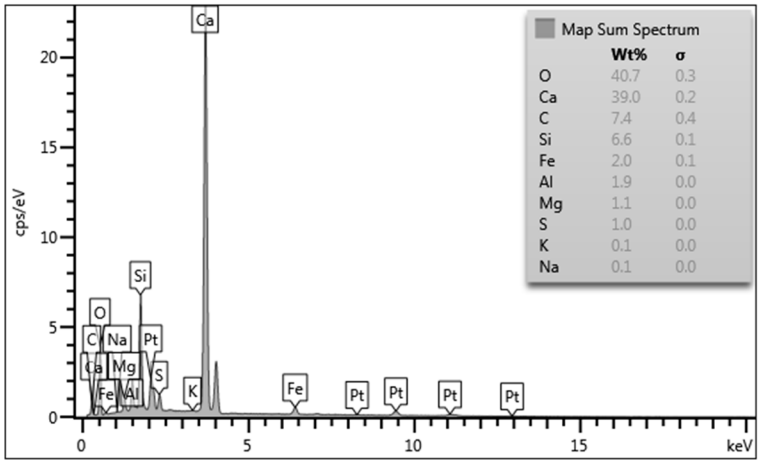

(**b**)

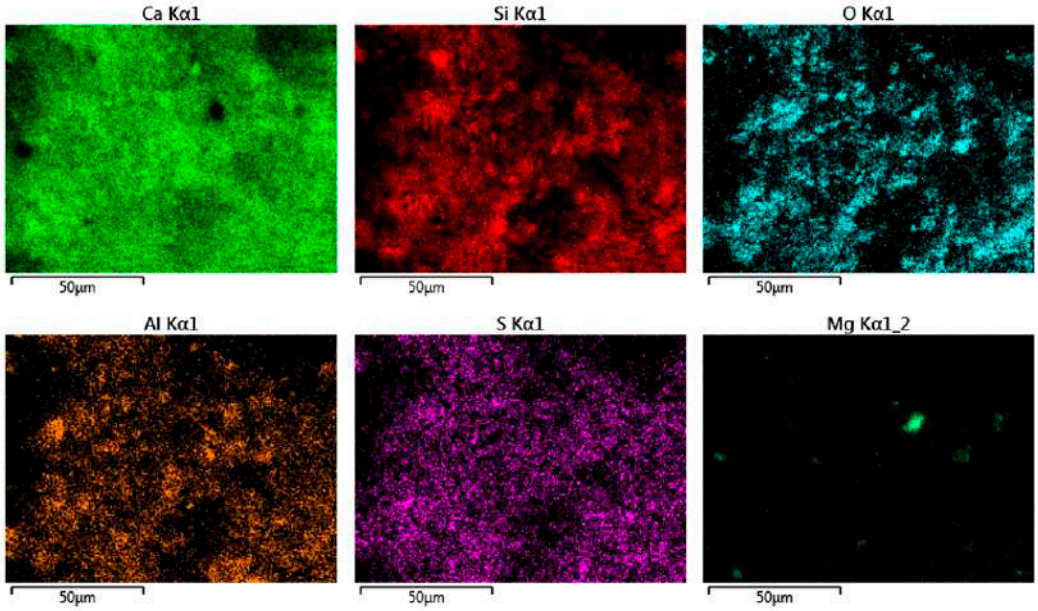

(**c**)

Figure 15. EDX maps of control concrete specimens (100% OPC) exposed to 800 °C: (**a**) electron image; (**b**) map sum spectrum; (**c**) layered elements images.

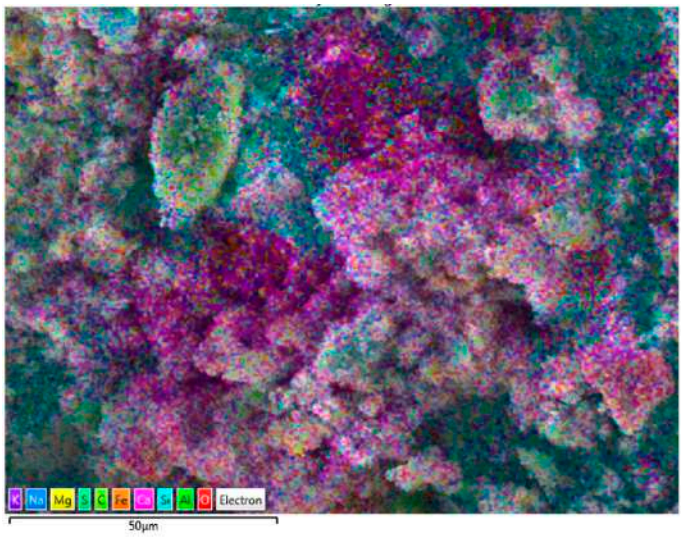

(**a**)

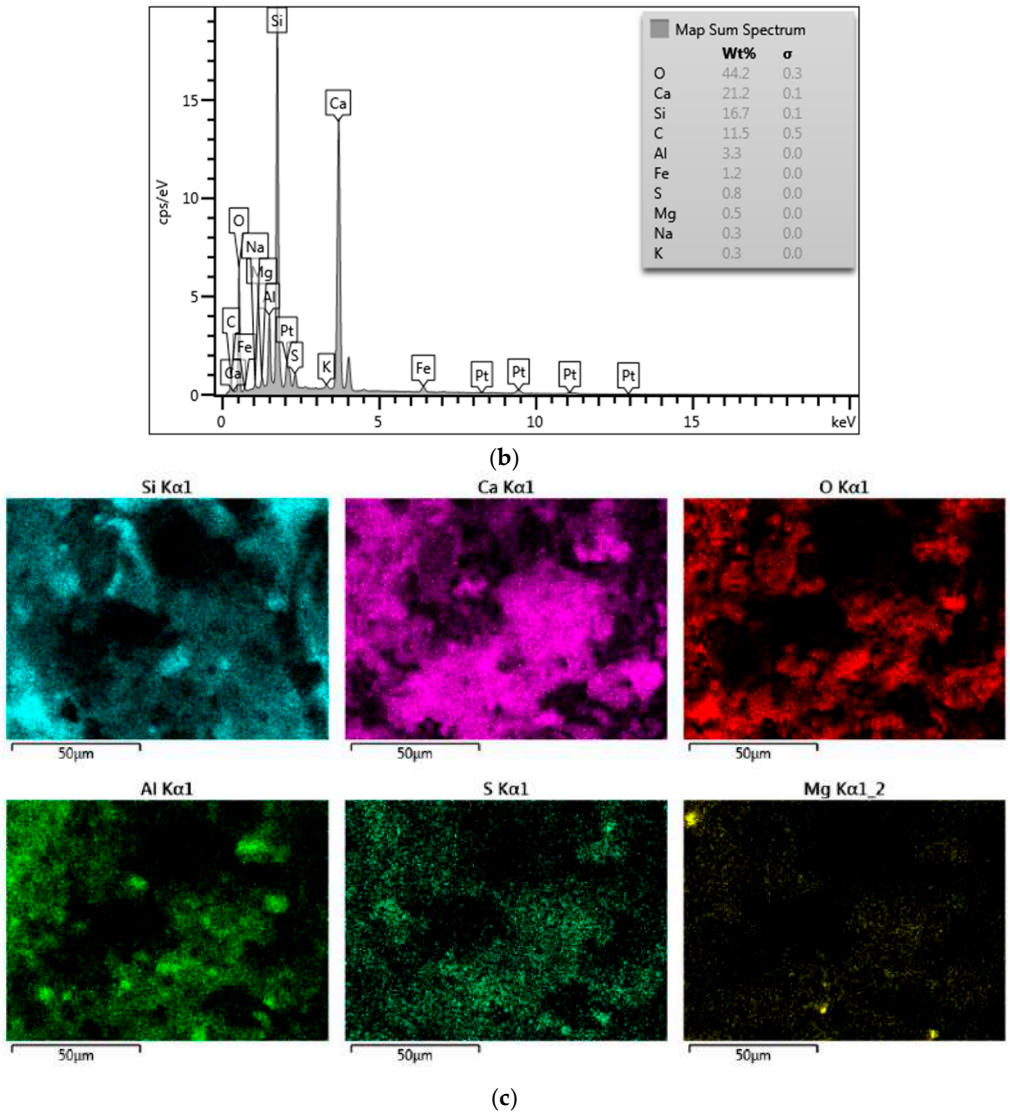

Figure 16. EDX maps of high level WTCPs-incorporated and 4% WGBNPs-supplemented concrete exposed to 800 °C: (**a**) electron image; (**b**) map sum spectrum; (**c**) layered elements images.

3.10. Thermogravimetric and Differential Thermal Analyser (TGA)

Figure 17 shows the analysis results of the TGA curves of modified concrete designed with a high amount of WTCP and WGBNPs. The effect of heating (200, 400, 600, and 800 °C) on the structure of 100% OPC, 60% WTCPs, 4% WGBNPs, and 6% WGBNPs mixtures were evaluated. The control specimens of 100% OPC were found to be lower stability under elevated temperatures compared to other specimens. It was observed that specimens made with 60% OPC replacement via WTCPs and WGBNPs inclusion had significantly high thermal stability under the heating. The change in weight was improved from 73.56% to 74.29%, 74.65%, and 80.61% with an additional 60% WTCPs and 4% and 6% WGBNPs in the matrix, respectively. The higher performance of 60% WTCPs, 4% WGBNPs, and 6% WGBNPs mixtures under an aggressive heating environment attributed to the low calcium content with higher silica and aluminium compared to the 100% OPC control mixture. The high loss in weight for the 100% OPC specimens may be due to the evaporation of free water when it was heated in the furnace. Additionally, the dehydration of cement gel could make the crystalline phases more dense [110].

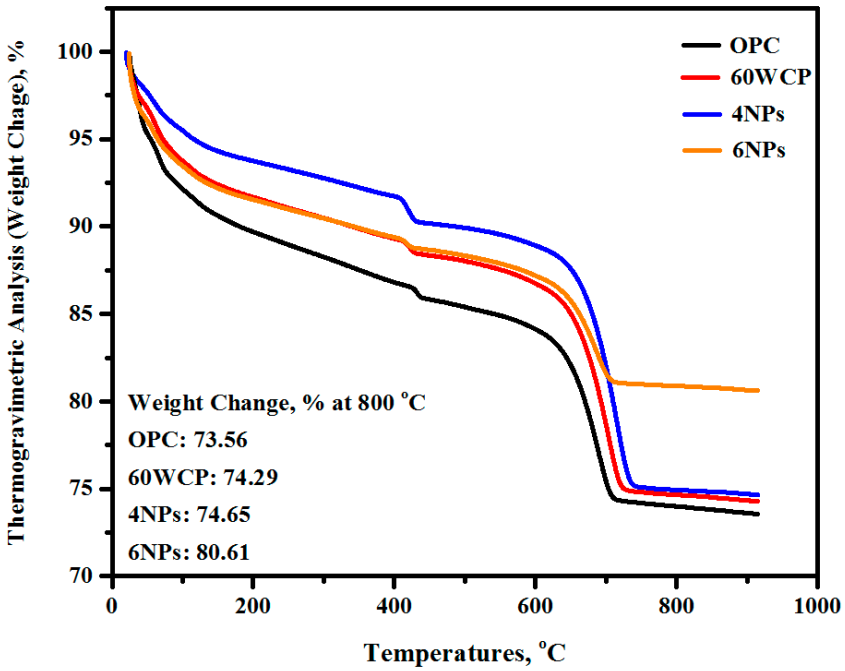

Figure 17. Weight change percentage of proposed concrete containing a high volume of ceramic and WGBNPs exposed to 900 °C.

3.11. FTIR Spectral Analyses of Specimens

Figure 18 illustrates the Fourier transform infrared spectroscopy (FTIR) of modified concrete containing a high amount of WTCPs and WGBNPs and exposed to elevated temperature (800 °C). The FTIR spectral analysis showed main bands around 600–1200 cm^{-1}. The stretching bands of Si-O-Al, Al-OH, and Si-O/C-(A)-S-H were located at a wavenumber of 650–700 cm^{-1}, 750–800 cm^{-1}, and 850–900 cm^{-1}, respectively. The changes in the band vibrations of varying modify concrete mixtures after exposure to heating were clearly evidenced. The change in the IR vibration frequency for the OPC specimen compared to the ones made using WTCPs and WGBNPs can be ascribed to the decrease in C-(A)-S-H gels in the exposed control specimens' matrix, which weakened the three-dimensional structure. The replacement of 60% OPC with WTCPs and WGBNPs reduced the production of C-(A)-S-H gels, displaying high performance under an aggressive heating environment.

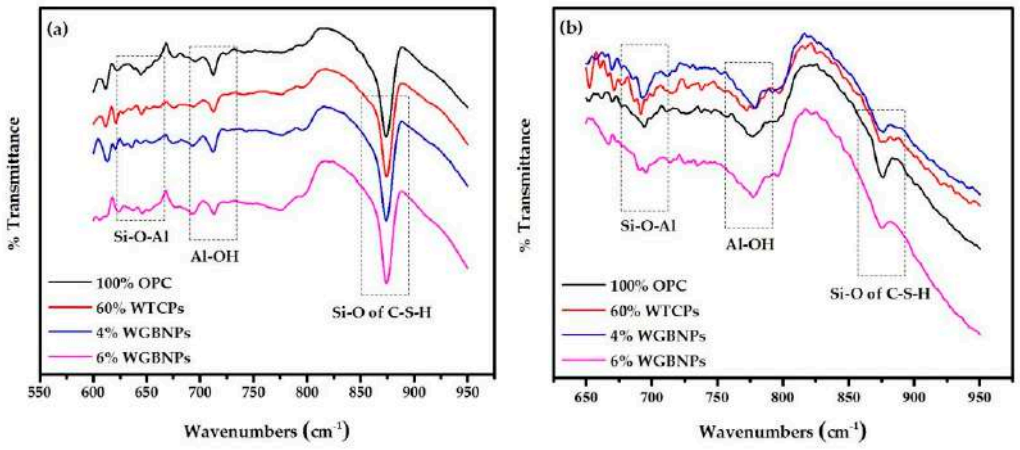

Figure 18. FTIR of modified concrete made from a high level of WTCPs and WGBNPs (**a**) before heating and (**b**) after being exposed to elevated temperatures (800 °C).

4. Modeling and Analysis

4.1. Predictive Equations

In this section, the behavior of a large amount of WTCPs-based concrete, incorporating WGBNPs exposed to elevated temperatures, was predicted based on strength loss, weight loss, and UPV using three quadratic equations. These equations aim to predict and assess the effect of varying amounts of WGBNPs (2–10%) on high-volume ceramic-based concrete subjected to heating ranging from 200 to 800 °C. Table 7 presents the developed equations, accompanied by several statistical parameters to ensure their accuracy and ability to provide precise predictions with minimal error. The robustness and the closeness with respect to the actual and predicted results of all equations were demonstrated by R^2 values higher than 0.97. This aligns with the findings of Mhaya, Algaifi [111], which highlight that an R^2 value higher than 0.9 indicates highly precise results. Moreover, the MAPE was calculated to evaluate the accuracy of the developed equations. Low MAPE values indicate excellent results, while high values indicate poor predictive performance. In our study, the MAPE values for strength loss, weight loss, and UPV were 7.46%, 2.268%, and 2.743%, respectively, confirming that the equations are reliable and accurate. These findings are consistent with those of Sujjaviriyasup and Pitiruek [112], who reported that higher accuracy could be obtained when the MAPE value is lower than 10%. Additionally, analysis of variance (ANOVA) was used to validate the performance of the proposed equations and their terms using *p*-values and F-values (Table 8). A higher F-value and a lower *p*-value (less than 0.05) indicate that the model and its terms are significant [113]. It was observed that the equations for strength loss, weight loss, and UPV, as well as their terms, are all significant.

Table 7. Predicted equations for strength loss, weight loss, and UPV.

Response	Developed Equations with Their Validations	
Strength loss (%)	$SL = 1.66 - 0.32X_1 - 0.004X_2 + 0.0001X_2^2$	
	$R^2 = 0.9993$	$MAPE = 7.46$
Weight loss (%)	$WL = -0.07 - 0.032X_1 + 0.0068X_2 - 0.0001X_1X_2 + 6.91E^{-6}X_2^2$	
	$R^2 = 0.9994$	$MAPE = 2.268$
UPV (m/s)	$UPV = 3135.2 + 266.5X_1 + 2.33X_2 - 21.76X_1^2 - 0.005X_2^2$	
	$R^2 = 0.9719$	$MAPE = 2.743$

Table 8. ANOVA analysis for the proposed equations.

Dependent Variables	Term	Mean Square	Sum of Squares	*p*-Value	F-Value	Note
SL	Model	1810.39	5431.2	<0.0001	2233.2	significant
	X_1	9.63	9.63	0.0183	11.88	
	X_2	5251.1	5251.1	<0.0001	6477.4	
	X_2^2	170.51	170.51	<0.0001	210.3	
WL	Model	22.92	91.69	<0.0001	1784.5	significant
	X_1	1.01	1.01	0.0009	78.84	
	X_2	89.78	89.78	<0.0001	6989.9	
	X_1X_2	0.116	0.116	0.0399	9	
	X_2^2	0.773	0.773	0.0015	60.18	
UPV	Model	9.25×10^5	3.69×10^6	0.0023	34.53	significant
	X_1	2773.5	2773.5	0.7637	0.1036	
	X_2	3.09×10^6	3.09×10^6	0.0004	115.44	
	X_1^2	2.42×10^5	2.42×10^5	0.0396	9.05	
	X_2^2	3.61×10^5	3.61×10^5	0.0213	13.50	

4.2. Relationship Between Dependent and Independent Variables

After developing three quadratic equations, 2D and 3D plots were constructed to clearly illustrate the evolution of CS, WL, and UPV with varying values of WGBNPs and temperature. These plots provide deep insights into the relationships between the independent and dependent variables of the proposed concrete. As shown in Figure 19, with the increase in WGBNPs, both strength and weight loss decreased, while the UPV improved. On the other hand, increasing the temperature led to a decrease in strength and UPV, as well as an increase in weight loss. However, at 6% WGBNPs, the proposed concrete exhibited reasonable results compared to the control sample. Specifically, at 200 °C, the strength, weight loss, and UPV were 3.1%, 1.18%, and 4352 m/s, respectively, compared to the control sample's 3.6%, 1.44%, and 3680 m/s. At 800 °C, these values were 62.4%, 8.95%, and 2604 m/s, respectively, compared to the control sample's 64.6%, 9.63%, and 2410 m/s.

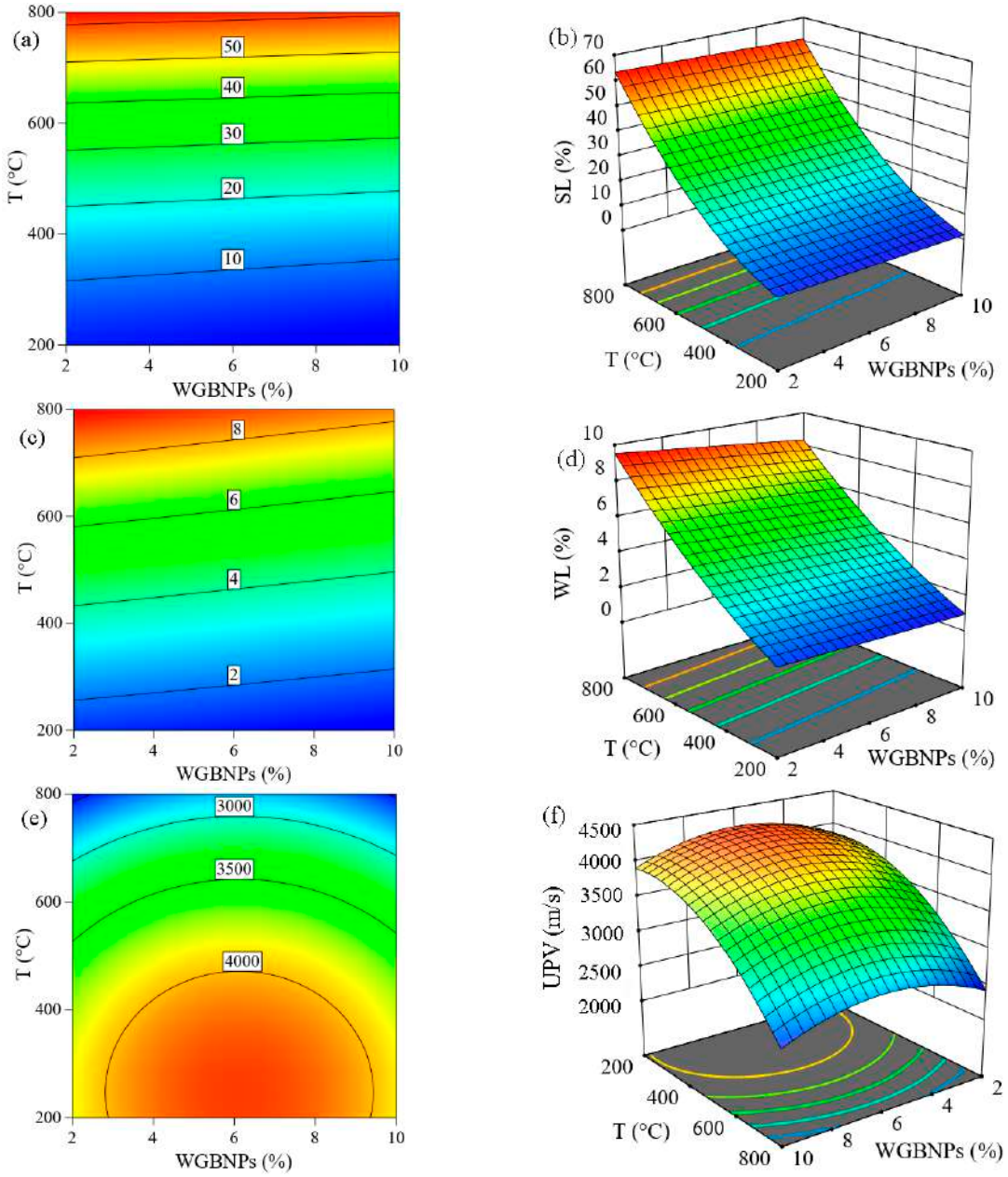

Figure 19. Evolution of the proposed concrete exposed to elevated temperature: (**a**,**b**) SL; (**c**,**d**) WL; (**e**,**f**) UPV.

4.3. Variables Interaction Analysis

In this section, the interaction of the independent variables involving WGBNPs (X_1) and temperature (X_2) and their impact on SL, WL, and UPV of the proposed concrete were investigated. As shown in Figure 20, the first variable (WGBNPs) showed a positive effect on strength and weight loss, indicated by a gradient slope. Specifically, both SL and WL decreased with the increase in WGBNPs content. Additionally, UPV increased with the increase in WGBNPs up to 6%; beyond this value, a decrease in UPV was observed. On the other hand, the second independent variable, temperature, exhibited a sharp slope, indicating that SL, WL, and UPV were negatively affected by the increasing temperature.

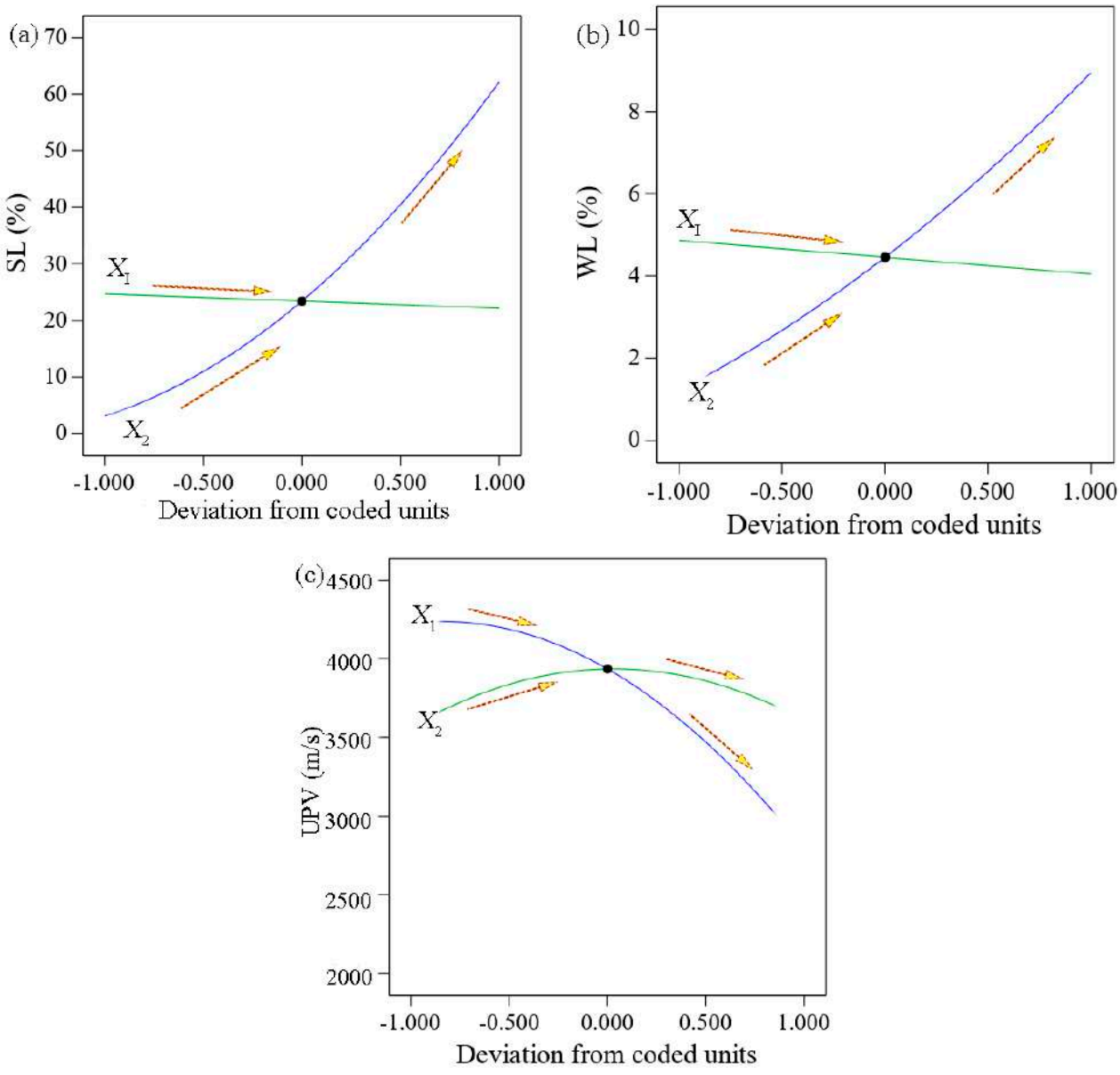

Figure 20. Perturbation plot for (**a**) SL, (**b**) WL, and (**c**) UPV.

4.4. Equations Verification

According to Algaifi, Syamsir [114], an additional experimental test should be conducted and compared with the predicted results to verify the accuracy and reliability of the developed equations. The difference between the experimental and predicted results (error percentage) should not exceed 10%, indicating a good agreement, as supported by

Salah, Mutalib [115]. Moreover, an equation's performance is considered excellent when the MAPE approaches zero. Equation (5) presents the error percentage formula used to verify the proposed equations.

In our study, as shown in Table 9, the MAPE for SL, WL, and UPV of the proposed equations are 5.6%, 3.8%, and 1.61%, respectively, demonstrating the equations' ability to forecast with minimal error.

$$Error\ percentage\,(\%) = \frac{Experimental - \Pr edicted}{Experimental} \times 100 \quad (5)$$

Table 9. Verification of the developed equations.

Output	Input		Experimental	Predicted	Error Percentage (%)
	WGBNPs, (%)	T, (°C)			
SL (%)	4	400	13.99	14.78	5.6
WL (%)	4	400	3.354	3.482	3.8
UPV (m/s)	4	400	4050	3985	1.61

5. Conclusions

Effects of WTCPs and WGBNPs content on the structural engineering properties of modified concrete were assessed with respect to elevated temperatures resistance. From the results, the following conclusions can be made:

i. From the obtained results, it is found the workability and compressive strength are significantly influenced by WTCPs and WGBNPs content. The slump value of fresh concrete mixtures tend to decrease with the increasing content of WTCPs and WGBNPs in the OPC matrix. However, the results showed that the added 4% of WGBNPs to the WTCPs-OPC matrix enhances the compressive strength performance among other ratios (2, 6, 8, and 10%).

ii. Replacement of 60% of OPC by WTCPs significantly improved the durability performance of the proposed concrete by decreasing the loss of compressive strength after exposure to the varying elevated temperatures (200, 400, 600, and 800 °C). It is well known that increasing the aluminosilicate content in the cement matrix increases its thermal stability.

iii. Varying the content of WGBNPs in the cement matrix considerably increased its resistance to heating by increasing the residual compressive strength and reducing the weight loss percentage.

iv. The UPV test results indicate that the inclusion of WTCPs and WGBNPs in the cement matrix controlled the internal cracks and pores number and enhanced the performance of the matrix under the heating.

v. The microstructures analyses using XRD, FTIR, FESEM, EDX, and TGA measurements demonstrated the good thermal stability of the modified concrete made from high-percentage WTCPs (60%) and WGBNPs when subjected to temperatures up to 800 °C.

vi. A practical benefit of examining the surface discoloration in fire-modified concrete that contains a high volume of WTCPs and WGBNPs lies in its use for the preliminary assessment of fire-related damage. This allows for a better understanding of the fire's intensity.

vii. It is asserted that reusing industrial materials like ceramic tiles and glass bottles can result in the production of highly durable concrete. This approach offers economic benefits, enhances sustainability, and promotes environmental friendliness.

Author Contributions: Conceptualization, Z.H.J. and A.M.M.; methodology, Z.H.J., A.M.M. and R.A.; software, H.A.A.; validation, Z.H.J., H.A.A. and T.X.; formal analysis, Z.H.J.; investigation, N.H.A.K.; resources, G.F.H.; data curation, Z.H.J.; writing—original draft preparation, Z.H.J.; writing—review and editing, Z.H.J., N.H.A.K. and G.F.H.; visualization, T.X.; supervision, N.H.A.K.; project administration, A.M.M. and R.A.; funding acquisition, G.F.H. All authors have read and agreed to the published version of the manuscript.

Funding: Universiti Teknologi Malaysia Fundamental Research (Q.J130000.3822.22H88 and R.J130000.7622.4C806).

Institutional Review Board Statement: Not applicable.

Informed Consent Statement: Not applicable.

Data Availability Statement: The original contributions presented in the study are included in the article, further inquiries can be directed to the corresponding author.

Acknowledgments: Authors thank Universiti Teknologi Malaysia for their support and cooperation in conducting this research. This research was supported and funded by the Universiti Teknologi Malaysia Fundamental Research (Q.J130000.3822.22H88 and R.J130000.7622.4C806).

Conflicts of Interest: The authors declare no conflicts of interest.

References

1. Ji, Z.; Zhang, G.; Liu, R.; Qu, J.; Liu, H. Potential applications of solid waste-based geopolymer materials: In wastewater treatment and greenhouse gas emission reduction. *J. Clean. Prod.* **2024**, *443*, 141144.
2. Rodriguez-Morales, J.; Burciaga-Diaz, O.; Gomez-Zamorano, L.Y.; Escalante-Garcia, J.I. Transforming construction and demolition waste concrete as a precursor in sustainable cementitious materials: An innovative recycling approach. *Resour. Conserv. Recycl.* **2024**, *204*, 107474.
3. Kubba, Z.; Samadi, M.; Huseien, G.F. Effects of recycled wastes ceramic as aggregates replacement on flexural behaviour of reinforced concrete beams. *AIP Conf. Proc.* **2023**, *2806*, 040038.
4. Kim, J.E.; Seo, J.; Yang, K.-H.; Kim, H.-K. Cost and CO_2 emission of concrete incorporating pretreated coal bottom ash as fine aggregate: A case study. *Constr. Build. Mater.* **2023**, *408*, 133706.
5. Chaudhury, R.; Sharma, U.; Thapliyal, P.; Singh, L. Low-CO_2 emission strategies to achieve net zero target in cement sector. *J. Clean. Prod.* **2023**, *417*, 137466.
6. Huseien, G.F.; Tang, W.; Yu, Y.; Wong, L.S.; Mirza, J.; Dong, K.; Gu, X. Evaluation of high-volume fly-ash cementitious binders incorporating nanosilica as eco-friendly sustainable concrete repair materials. *Constr. Build. Mater.* **2024**, *447*, 138022.
7. Younas, H.; Yu, J.; Leung, C.K. Mechanical and environmental performance of high-strength strain-hardening cementitious composites with high-dosage ternary supplementary cementitious materials: Fly ash, limestone, and calcined clay. *Constr. Build. Mater.* **2024**, *444*, 137856.
8. Nazeer, M.; Kapoor, K.; Singh, S. Strength, durability and microstructural investigations on pervious concrete made with fly ash and silica fume as supplementary cementitious materials. *J. Build. Eng.* **2023**, *69*, 106275.
9. Yaseen, N. Exploring the potential of sugarcane bagasse ash as a sustainable supplementary cementitious material: Experimental investigation and statistical analysis. *Results Chem.* **2024**, *10*, 101723.
10. Mhaya, A.M.; Huseien, G.F.; Faridmehr, I.; Abidin, A.R.Z.; Alyousef, R.; Ismail, M. Evaluating mechanical properties and impact resistance of modified concrete containing ground Blast Furnace slag and discarded rubber tire crumbs. *Constr. Build. Mater.* **2021**, *295*, 123603.
11. Chen, H.; Yang, J. A new supplementary cementitious material: Walnut shell ash. *Constr. Build. Mater.* **2023**, *408*, 133852.
12. Amin, M.N.; Khan, K.; Arab, A.M.A.; Farooq, F.; Eldin, S.M.; Javed, M.F. Prediction of sustainable concrete utilizing rice husk ash (RHA) as supplementary cementitious material (SCM): Optimization and hyper-tuning. *J. Mater. Res. Technol.* **2023**, *25*, 1495–1536.
13. Shi, C.; Qian, X.; Yin, J.; Gautam, B.; Hu, C. Synergistic performance enhancement of cementitious materials by co-incorporation of waste brick powder and limestone powder. *Constr. Build. Mater.* **2024**, *436*, 136893.
14. Borinaga-Treviño, R.; Cuadrado, J.; Canales, J.; Rojí, E. Lime mud waste from the paper industry as a partial replacement of cement in mortars used on radiant floor heating systems. *J. Build. Eng.* **2021**, *41*, 102408.
15. Nunes, G.M.; Anjos, M.A.; Lins, A.B.S.; Negreiros, A.M.S.; Pessoa, L.R. Evaluation of the mechanical behaviour of representative volumetric elements of 3DCP masonry mixtures with partial replacement of cement by limestone filler and metakaolin. *J. Build. Eng.* **2023**, *78*, 107650.
16. Mhaya, A.M.; Baharom, S.; Baghban, M.H.; Nehdi, M.L.; Faridmehr, I.; Huseien, G.F.; Algaifi, H.A.; Ismail, M. Systematic experimental assessment of POFA concrete incorporating waste tire rubber aggregate. *Polymers* **2022**, *14*, 2294.
17. Al Shouny, A.; Issa, U.H.; Miky, Y.; Sharaky, I.A. Evaluating and selecting the best sustainable concrete mixes based on recycled waste materials. *Case Stud. Constr. Mater.* **2023**, *19*, e02382.

18. Huseien, G.F.; Mirza, J.; Ismail, M.; Ghoshal, S.; Hussein, A.A. Geopolymer mortars as sustainable repair material: A comprehensive review. *Renew. Sustain. Energy Rev.* **2017**, *80*, 54–74.
19. Abera, Y.S.A. Performance of concrete materials containing recycled aggregate from construction and demolition waste. *Results Mater.* **2022**, *14*, 100278.
20. Bheel, N.; Chohan, I.M.; Ghoto, A.A.; Abbasi, S.A.; Tag-eldin, E.M.; Almujibah, H.R.; Ahmad, M.; Benjeddou, O.; Gonzalez-Lezcano, R.A. Synergistic effect of recycling waste coconut shell ash, metakaolin, and calcined clay as supplementary cementitious material on hardened properties and embodied carbon of high strength concrete. *Case Stud. Constr. Mater.* **2024**, *20*, e02980.
21. Samadi, M.; Huseien, G.F.; Mohammadhosseini, H.; Lee, H.S.; Lim, N.H.A.S.; Tahir, M.M.; Alyousef, R. Waste ceramic as low cost and eco-friendly materials in the production of sustainable mortars. *J. Clean. Prod.* **2020**, *266*, 121825.
22. Huseien, G.F.; Sam, A.R.M.; Shah, K.W.; Asaad, M.A.; Tahir, M.M.; Mirza, J. Properties of ceramic tile waste based alkali-activated mortars incorporating GBFS and fly ash. *Constr. Build. Mater.* **2019**, *214*, 355–368.
23. Sabbrojjaman, M.; Liu, Y.; Tafsirojjaman, T. A comparative review on the utilisation of recycled waste glass, ceramic and rubber as fine aggregate on high performance concrete: Mechanical and durability properties. *Dev. Built Environ.* **2024**, *17*, 100371.
24. Naenudon, S.; Wongsa, A.; Ekprasert, J.; Sata, V.; Chindaprasirt, P. Enhancing the properties of fly ash-based geopolymer concrete using recycled aggregate from waste ceramic electrical insulator. *J. Build. Eng.* **2023**, *68*, 106132.
25. Chen, X.; Zhang, D.; Cheng, S.; Xu, X.; Zhao, C.; Wang, X.; Wu, Q.; Bai, X. Sustainable reuse of ceramic waste powder as a supplementary cementitious material in recycled aggregate concrete: Mechanical properties, durability and microstructure assessment. *J. Build. Eng.* **2022**, *52*, 104418.
26. Zegardło, B. Heat-resistant concretes containing waste carbon fibers from the sailing industry and recycled ceramic aggregates. *Case Stud. Constr. Mater.* **2022**, *16*, e01084.
27. Robayo-Salazar, R.; Valencia-Saavedra, W.; De Gutiérrez, R.M. Recycling of concrete, ceramic, and masonry waste via alkaline activation: Obtaining and characterization of hybrid cements. *J. Build. Eng.* **2022**, *46*, 103698.
28. Nepomuceno, M.C.; Isidoro, R.A.; Catarino, J.P. Mechanical performance evaluation of concrete made with recycled ceramic coarse aggregates from industrial brick waste. *Constr. Build. Mater.* **2018**, *165*, 284–294.
29. Rashid, K.; Razzaq, A.; Ahmad, M.; Rashid, T.; Tariq, S. Experimental and analytical selection of sustainable recycled concrete with ceramic waste aggregate. *Constr. Build. Mater.* **2017**, *154*, 829–840.
30. Huseien, G.F.; Sam, A.R.M.; Shah, K.W.; Mirza, J. Effects of ceramic tile powder waste on properties of self-compacted alkali-activated concrete. *Constr. Build. Mater.* **2020**, *236*, 117574.
31. Jiang, X.; Xiao, R.; Zhang, M.; Hu, W.; Bai, Y.; Huang, B. A laboratory investigation of steel to fly ash-based geopolymer paste bonding behavior after exposure to elevated temperatures. *Constr. Build. Mater.* **2020**, *254*, 119267.
32. Samadi, M.; Hussin, M.W.; Lee, H.S.; Sam, A.R.M.; Ismail, M.A.; Lim, N.H.A.S.; Ariffin, N.F.; Khalid, N.H.A. Properties of mortar containing ceramic powder waste as cement replacement. *J. Teknol.* **2015**, *77*, 93–97.
33. Zhou, W.; Yan, C.; Duan, P.; Liu, Y.; Zhang, Z.; Qiu, X.; Li, D. A comparative study of high-and low-Al_2O_3 fly ash based-geopolymers: The role of mix proportion factors and curing temperature. *Mater. Des.* **2016**, *95*, 63–74.
34. Yusuf, M.O. Performance of slag blended alkaline activated palm oil fuel ash mortar in sulfate environments. *Constr. Build. Mater.* **2015**, *98*, 417–424.
35. Huseien, G.F.; Mirza, J.; Ismail, M.; Hussin, M.W.; Arrifin, M.; Hussein, A. The Effect of Sodium Hydroxide Molarity and Other Parameters on Water Absorption of Geopolymer Mortars. *Indian J. Sci. Technol.* **2016**, *9*, 1–7.
36. Huseien, G.F.; Ismail, M.; Tahir, M.M.; Mirza, J.; Khalid, N.H.A.; Asaad, M.A.; Husein, A.A.; Sarbini, N.N. Synergism between palm oil fuel ash and slag: Production of environmental-friendly alkali activated mortars with enhanced properties. *Constr. Build. Mater.* **2018**, *170*, 235–244.
37. Zhang, B.; Zhu, H.; Cheng, Y.; Huseien, G.F.; Shah, K.W. Shrinkage mechanisms and shrinkage-mitigating strategies of alkali-activated slag composites: A critical review. *Constr. Build. Mater.* **2022**, *318*, 125993.
38. Huseien, G.F.; Sam, A.R.M.; Mirza, J.; Tahir, M.M.; Asaad, M.A.; Ismail, M.; Shah, K.W. Waste ceramic powder incorporated alkali activated mortars exposed to elevated Temperatures: Performance evaluation. *Constr. Build. Mater.* **2018**, *187*, 307–317.
39. Huseien, G.F.; Mirza, J.; Ismail, M.; Hussin, M.W. Influence of different curing temperatures and alkali activators on properties of GBFS geopolymer mortars containing fly ash and palm-oil fuel ash. *Constr. Build. Mater.* **2016**, *125*, 1229–1240.
40. Hossain, M.; Karim, M.; Hossain, M.; Islam, M.; Zain, M.F.M. Durability of mortar and concrete containing alkali-activated binder with pozzolans: A review. *Constr. Build. Mater.* **2015**, *93*, 95–109.
41. Hussein, A.A.; Jaya, R.P.; Hassan, N.A.; Yaacob, H.; Huseien, G.F.; Ibrahim, M.H.W. Performance of nanoceramic powder on the chemical and physical properties of bitumen. *Constr. Build. Mater.* **2017**, *156*, 496–505.
42. Huseien, G.F.; Mirzaa, J.; Ismaila, M.; Hussina, M.W.; Ariffina, M.A.M. Potential use coconut milk as alternative to alkali solution for geopolymer production. *J. Teknol.* **2016**, *78*, 133–139.
43. Harada, T.; Takeda, J.; Yamane, S.; Furumura, F. Strength, elasticity and thermal properties of concrete subjected to elevated temperatures. *Spec. Publ.* **1972**, *34*, 377–406.
44. Morley, P.; Royles, R. Response of the bond in reinforced concrete to high temperatures. *Mag. Concr. Res.* **1983**, *35*, 67–74.
45. Kodur, V. Properties of concrete at elevated temperatures. *ISRN Civ. Eng.* **2014**, *2014*, 468510.
46. Novak, J.; Kohoutkova, A. Mechanical properties of concrete composites subject to elevated temperature. *Fire Saf. J.* **2018**, *95*, 66–76.

47. Buchanan, A.H.; Abu, A.K. *Structural Design for Fire Safety*; John Wiley & Sons: Hoboken, NJ, USA, 2017.
48. Awal, A.A.; Shehu, I. Performance evaluation of concrete containing high volume palm oil fuel ash exposed to elevated temperature. *Constr. Build. Mater.* **2015**, *76*, 214–220.
49. Saavedra, W.G.V.; de Gutiérrez, R.M. Performance of geopolymer concrete composed of fly ash after exposure to elevated temperatures. *Constr. Build. Mater.* **2017**, *154*, 229–235.
50. M. Mhaya, A.; Baghban, M.H.; Faridmehr, I.; Huseien, G.F.; Abidin, A.R.Z.; Ismail, M. Performance evaluation of modified rubberized concrete exposed to aggressive environments. *Materials* **2021**, *14*, 1900.
51. Ismail, M.; Ismail, M.E.; Muhammad, B. Influence of elevated temperatures on physical and compressive strength properties of concrete containing palm oil fuel ash. *Constr. Build. Mater.* **2011**, *25*, 2358–2364.
52. Omer, S.A.; Demirboga, R.; Khushefati, W.H. Relationship between compressive strength and UPV of GGBFS based geopolymer mortars exposed to elevated temperatures. *Constr. Build. Mater.* **2015**, *94*, 189–195.
53. Ranjbar, N.; Mehrali, M.; Alengaram, U.J.; Metselaar, H.S.C.; Jumaat, M.Z. Compressive strength and microstructural analysis of fly ash/palm oil fuel ash based geopolymer mortar under elevated temperatures. *Constr. Build. Mater.* **2014**, *65*, 114–121.
54. Muhedin, D.A.; Ibrahim, R.K. Effect of waste glass powder as partial replacement of cement & sand in concrete. *Case Stud. Constr. Mater.* **2023**, *19*, e02512.
55. Nodehi, M.; Ren, J.; Shi, X.; Debbarma, S.; Ozbakkaloglu, T. Experimental evaluation of alkali-activated and portland cement-based mortars prepared using waste glass powder in replacement of fly ash. *Constr. Build. Mater.* **2023**, *394*, 132124.
56. Subhani, M.; Ali, S.; Allan, R.; Grace, A.; Rahman, M. Physical and mechanical properties of self-compacting geopolymer concrete with waste glass as partial replacement of fine aggregate. *Constr. Build. Mater.* **2024**, *437*, 136956.
57. Paul, D.; Bindhu, K.; Matos, A.M.; Delgado, J. Eco-friendly concrete with waste glass powder: A sustainable and circular solution. *Constr. Build. Mater.* **2022**, *355*, 129217.
58. Shi, C.; Zheng, K. A review on the use of waste glasses in the production of cement and concrete. *Resour. Conserv. Recycl.* **2007**, *52*, 234–247.
59. Franco-Luján, V.; Ramírez-Arellanes, S.; Gomez-Sanchez, A.; Pérez-Ramos, A.; Cruz-García, E.; Cruz-Martínez, H. Properties of fresh and hardened cement-based materials with waste glass as supplementary cementitious material: A review. *J. Build. Eng.* **2024**, *95*, 110137.
60. Dai, T.; Fang, C.; Liu, T.; Zheng, S.; Lei, G.; Jiang, G. Waste glass powder as a high temperature stabilizer in blended oil well cement pastes: Hydration, microstructure and mechanical properties. *Constr. Build. Mater.* **2024**, *439*, 137359.
61. Xi, X.; Zheng, Y.; Zhuo, J.; Zhang, P.; Golewski, G.L.; Du, C. Influence of water glass modulus and alkali content on the properties of alkali-activated thermally activated recycled cement. *Constr. Build. Mater.* **2024**, *452*, 138867.
62. Geng, C.; Wu, X.; Yao, X.; Wang, C.; Mei, Z.; Jiang, T. Reusing waste glass powder to improve the strength stability of cement at HTHP. *J. Pet. Sci. Eng.* **2022**, *213*, 110394.
63. Kim, J.; Yi, C.; Zi, G. Waste glass sludge as a partial cement replacement in mortar. *Constr. Build. Mater.* **2015**, *75*, 242–246.
64. Khan, M.N.N.; Saha, A.K.; Sarker, P.K. Reuse of waste glass as a supplementary binder and aggregate for sustainable cement-based construction materials: A review. *J. Build. Eng.* **2020**, *28*, 101052.
65. Khmiri, A.; Samet, B.; Chaabouni, M. Assessment of the waste glass powder pozzolanic activity by different methods. *Int. J. Res. Rev. Appl. Sci.* **2012**, *10*, 322–328.
66. Madandoust, R.; Ghavidel, R. Mechanical properties of concrete containing waste glass powder and rice husk ash. *Biosyst. Eng.* **2013**, *116*, 113–119.
67. Aliabdo, A.A.; Abd Elmoaty, M.; Aboshama, A.Y. Utilization of waste glass powder in the production of cement and concrete. *Constr. Build. Mater.* **2016**, *124*, 866–877.
68. Kazmi, D.; Williams, D.J.; Serati, M. Waste glass in civil engineering applications—A review. *Int. J. Appl. Ceram. Technol.* **2020**, *17*, 529–554.
69. Silvestre, J.; Silvestre, N.; De Brito, J. Review on concrete nanotechnology. *Eur. J. Environ. Civ. Eng.* **2016**, *20*, 455–485.
70. Luo, Z.; Li, W.; Tam, V.W.; Xiao, J.; Shah, S.P. Current progress on nanotechnology application in recycled aggregate concrete. *J. Sustain. Cem. Based Mater.* **2019**, *8*, 79–96.
71. Hanus, M.J.; Harris, A.T. Nanotechnology innovations for the construction industry. *Prog. Mater. Sci.* **2013**, *58*, 1056–1102.
72. Hamzah, H.K.; Huseien, G.F.; Asaad, M.A.; Georgescu, D.P.; Ghoshal, S.; Alrshoudi, F. Effect of waste glass bottles-derived nanopowder as slag replacement on mortars with alkali activation: Durability characteristics. *Case Stud. Constr. Mater.* **2021**, *15*, e00775.
73. Huseien, G.F.; Faridmehr, I.; Nehdi, M.L.; Abadel, A.A.; Aiken, T.A.; Ghoshal, S. Structure, morphology and compressive strength of Alkali-activated mortars containing waste bottle glass nanoparticles. *Constr. Build. Mater.* **2022**, *342*, 128005.
74. Samadi, M.; Huseien, G.F.; Lim, N.H.A.S.; Mohammadhosseini, H.; Alyousef, R.; Mirza, J.; Abd Rahman, A.B. Enhanced performance of nano-palm oil ash-based green mortar against sulphate environment. *J. Build. Eng.* **2020**, *32*, 101640.
75. Onaizi, A.M.; Huseien, G.F.; Shukor Lim, N.H.A.; Tang, W.; Alhassan, M.; Samadi, M. Effective microorganisms and glass nanopowders from waste bottle inclusion on early strength and microstructure properties of high-volume fly-ash-based concrete. *Biomimetics* **2022**, *7*, 190.
76. *ASTM C 33*; Standard Specification for Concrete Aggregates. American Society for Testing and Materials: Philadelphia, PA, USA, 2003.

77. *ASTM C150*; Standard Specification for Portland Cement. American Society for Testing and Materials: West Conshohocken, PA, USA, 2001.
78. *ASTM C618-22*; Standard Specification for Coal Fly Ash and Raw or Calcined Natural Pozzolan for Use in Concrete. ASTM International: West Conshohocken, PA, USA, 2012; p. 1-4.
79. *ASTM C136-06*; Standard Test Method for Sieve Analysis of Fine and Coarse Aggregates. ASTM International: West Conshohocken, PA, USA, 2006.
80. Canadian Sociological Association. *Relative Density, and Absorption of Coarse Aggregate: Concrete Materials and Methods of Concrete Construction—Methods of Tests for Concrete*; CSA: Mississauga, ON, USA, 2019; Volume 23, p. 2-12A.
81. *ASTM C128-22*; Standard Test Method for Relative Density (Specific Gravity) and Absorption of Fine Aggregate. ASTM International: West Conshohocken, PA, USA, 2015; Volume 1, pp. 2–7.
82. *ASTM C579-96*; Standard Test Methods for Compressive Strength of Chemical-Resistant Mortars. Grouts, Monolithic Surfacings, and Polymer Concretes. ASTM International: West Conshohocken, PA, USA, 2001.
83. *ASTM C143*; Standard Test Method for Slump of Hydraulic-Cement Concrete. ASTM International: West Conshohocken, PA, USA, 2015.
84. *BS8110*; Structural Use of Concrete. British Standard: London, UK, 1986.
85. *ASTM E119*; Standard Test Methods for Fire Tests of Building Construction and Materials. ASTM: Philadelphia, PA, USA, 2012.
86. *ASTM C109/C109-20*; Standard Test Method for Compressive Strength of Hydraulic Cement Mortars (Using 2-in. or [50-mm] Cube Specimens). ASTM International: West Conshohocken, PA, USA, 2009.
87. *ASTM C109/C109M-20*; Standard Test Method for Pulse Velocity Through Concrete.. ASTM International: West Conshohocken, PA, USA, 2013.
88. *ISO/TR 834-3:1994*; Fire-Resistance Tests: Elements of Building Construction. Commentary on Test Method and Test Data Application. International Organization for Standardization: Geneva, Switzerland, 1994.
89. Algaifi, H.A.; Khan, M.I.; Shahidan, S.; Fares, G.; Abbas, Y.M.; Huseien, G.F.; Salami, B.A.; Alabduljabbar, H. Strength and acid resistance of ceramic-based self-compacting alkali-activated concrete: Optimizing and predicting assessment. *Materials* **2021**, *14*, 6208.
90. Ray, S.; Haque, M.; Ahmed, T.; Nahin, T.T. Comparison of artificial neural network (ANN) and response surface methodology (RSM) in predicting the compressive and splitting tensile strength of concrete prepared with glass waste and tin (Sn) can fiber. *J. King Saud Univ. Eng. Sci.* **2023**, *35*, 185–199.
91. Liu, K.; Zhang, L.; Wang, W.; Zhang, G.; Xu, L.; Fan, D.; Yu, R. Development of compressive strength prediction platform for concrete materials based on machine learning techniques. *J. Build. Eng.* **2023**, *80*, 107977.
92. Huseien, G.F.; Hamzah, H.K.; Sam, A.R.; Khalid, N.H.; Shah, K.W.; Deogrescu, D.P.; Mirza, J. Alkali-activated mortars blended with glass bottle waste nano powder: Environmental benefit and sustainability. *J. Clean. Prod.* **2020**, *243*, 118636.
93. Huseien, G.F. A Review on Concrete Composites Modified with Nanoparticles. *J. Compos. Sci.* **2023**, *7*, 67.
94. Onaizi, A.M.; Lim, N.H.A.S.; Huseien, G.F.; Amran, M.; Ma, C.K. Effect of the addition of nano glass powder on the compressive strength of high volume fly ash modified concrete. *Mater. Today Proc.* **2022**, *48*, 1789–1795.
95. Samadi, M.; Shah, K.W.; Huseien, G.F.; Lim, N.H.A.S. Influence of glass silica waste nano powder on the mechanical and microstructure properties of alkali-activated mortars. *Nanomaterials* **2020**, *10*, 324.
96. Yoo, D.-Y.; Oh, T.; Banthia, N. Nanomaterials in ultra-high-performance concrete (UHPC)–A review. *Cem. Concr. Compos.* **2022**, *134*, 104730.
97. Huseien, G.F.; Shah, K.W.; Sam, A.R.M. Sustainability of nanomaterials based self-healing concrete: An all-inclusive insight. *J. Build. Eng.* **2019**, *23*, 155–171.
98. Shao, Q.; Zheng, K.; Zhou, X.; Zhou, J.; Zeng, X. Enhancement of nano-alumina on long-term strength of Portland cement and the relation to its influences on compositional and microstructural aspects. *Cem. Concr. Compos.* **2019**, *98*, 39–48.
99. Li, W.; Li, X.; Chen, S.J.; Long, G.; Liu, Y.M.; Duan, W.H. Effects of nanoalumina and graphene oxide on early-age hydration and mechanical properties of cement paste. *J. Mater. Civ. Eng.* **2017**, *29*, 04017087.
100. Zhou, W.; Mo, J.; Xiang, S.; Zeng, L. Impact of elevated temperatures on the mechanical properties and microstructure of waste rubber powder modified polypropylene fiber reinforced concrete. *Constr. Build. Mater.* **2023**, *392*, 131982.
101. Mhaya, A.M.; Huseien, G.F.; Abidin, A.R.Z.; Ismail, M. Long-term mechanical and durable properties of waste tires rubber crumbs replaced GBFS modified concretes. *Constr. Build. Mater.* **2020**, *256*, 119505.
102. Zhang, P.; Sun, Y.; Wu, J.; Hong, J.; Gao, Z. Mechanical properties and microstructure of nano-modified geopolymer concrete containing hybrid fibers after exposure to elevated temperature. *Constr. Build. Mater.* **2023**, *409*, 134044.
103. Kantarci, F.; Türkmen, İ.; Ekinci, E. Improving elevated temperature performance of geopolymer concrete utilizing nano-silica, micro-silica and styrene-butadiene latex. *Constr. Build. Mater.* **2021**, *286*, 122980.
104. Tahwia, A.M.; Abd Ellatief, M.; Bassioni, G.; Heniegal, A.M.; Abd Elrahman, M. Influence of high temperature exposure on compressive strength and microstructure of ultra-high performance geopolymer concrete with waste glass and ceramic. *J. Mater. Res. Technol.* **2023**, *23*, 5681–5697.
105. Wong, L.S. Durability performance of geopolymer concrete: A review. *Polymers* **2022**, *14*, 868.
106. Huseien, G.F.; Tahir, M.M.; Mirza, J.; Ismail, M.; Shah, K.W.; Asaad, M.A. Effects of POFA replaced with FA on durability properties of GBFS included alkali activated mortars. *Constr. Build. Mater.* **2018**, *175*, 174–186.

107. Yu, M.; Wang, T.; Chi, Y.; Li, D.; Li, L.-Y.; Shi, F. Residual mechanical properties of GGBS-FA-SF blended geopolymer concrete after exposed to elevated temperatures. *Constr. Build. Mater.* **2024**, *411*, 134378.
108. Çelikten, S.; Atabey, İ.İ.; Bayer Öztürk, Z. Cleaner environment approach by the utilization of ceramic sanitaryware waste in Portland cement mortar at ambient and elevated temperatures. *Iran. J. Sci. Technol. Trans. Civ. Eng.* **2022**, *46*, 4291–4301.
109. Praneedpolkrang, P.; Chaiwasee, N.; Koedmontree, P.; Suthiwong, A.; Kaur, H.; Jaturapitakkul, C.; Tangchirapat, W. Effects of elevated temperature on mechanical properties and microstructures of alkali-activated mortar made from low calcium fly ash-calcium carbide residue mixture. *Case Stud. Constr. Mater.* **2024**, *21*, e03520.
110. Lima, V.M.; Basto, P.A.; Henrique, M.A.; Almeida, Y.M.; de Melo Neto, A.A. Optimizing the concentration of Na2O in alkaline activators to improve mechanical properties and reduce costs and CO_2 emissions in alkali-activated mixtures. *Constr. Build. Mater.* **2022**, *344*, 128185.
111. Mhaya, A.M.; Algaifi, H.A.; Shahidan, S.; Zuki, S.S.M.; Azmi, M.A.M.; Ibrahim, M.H.W.; Huseien, G.F. Systematic Evaluation of Permeability of Concrete Incorporating Coconut Shell as Replacement of Fine Aggregate. *Materials* **2022**, *15*, 7944.
112. Sujjaviriyasup, T.; Pitiruek, K. A hybridization of MODWT-SVR-DE model emphasizing on noise reduction and optimal parameter selection for prediction of CO2 emission in Thailand. *Cogent Eng.* **2024**, *11*, 2317540.
113. Algaifi, H.A.; Syamsir, A.; Baharom, S.; Alrshoudi, F.; Qaid, A.; Al-Fakih, A.M.; Mhaya, A.M.; Salah, H.A. Assessment of acoustic and mechanical properties in modified rubberized concrete. *Case Stud. Constr. Mater.* **2024**, *20*, e03063.
114. Algaifi, H.A.; Syamsir, A.; Baharom, S.; Sallah, H.A.; Anggraini, V.; Al-Fakih, A.M. Mathematical and Experimental Insights into Acid-Resistant Enhancements: Graphene Plates' Influence on Rubber-Incorporated Cementitious Materials. *J. Build. Eng.* **2024**, *95*, 110054.
115. Salah, H.A.; Mutalib, A.A.; Kaish, A.; Syamsir, A.; Algaifi, H.A. Development of Ultra-High-Performance Silica Fume-Based Mortar Incorporating Graphene Nanoplatelets for 3-Dimensional Concrete Printing Application. *Buildings* **2023**, *13*, 1949.